Superconductor - Semiconductor Quantum Dots in InAs/Al Nanowires for Majorana based Quantum Information

A Thesis presented
by
Deividas Sabonis
to
University of Copenhagen, Niels Bohr Institute

in partial fulfillment of the requirements
for the degree of Master of Science
in the subject of
Physics

University of Copenhagen
Copenhagen, Denmark
August 2017

Thesis advisor: Prof. Charles M. Marcus Deividas Sabonis

Superconductor - Semiconductor Quantum Dots in InAs/Al Nanowires for Majorana based Quantum Information

Abstract

After the first demonstration in 2012 of what is now called the first ever signatures of the Majorana bound states in a condensed matter system, different groups set up experiments to test the effect in the same or very similar solid state systems. After a few more demonstrations of the transport signatures compatible with Majorana bound states the community naturally started aiming for the first steps towards employing the observed Majorana bound states for quantum information purposes. Majorana bound states based approach to quantum computation is known under the name of topological quantum computing. Even though this approach promises to have a natural protection of quantum states against decoherence it might also be affected by various physical processes that change the parity of the superconductor. Protection against such errors requires qubit manipulations on a time scale shorter than the typical poisoning time of the system but on a time scale longer than any residual Majorana overlap or charging energy dominant splitting.

My contribution in this thesis further investigates these hybrid structures as a potential future platform for topological quantum information processing applications. I demonstrate the control and tuning of superconducting islands defined by electrostatic gates in one dimensional nanowires. Also the technical preparation and the steps necessary to achieve the manipulation of the Majorana based qubit are outlined. The methods reported use both slow - DC and fast - RF charge sensing of an isolated superconducting island. Charge sensing is done by capacitively coupling the island to a sensor dot - a proximal nanowire. The characterization of devices, building and the integration, both software-wise and hardware-wise, and testing of the fast data acquisition setup forms the cornerstone behind this thesis.

Contents

Listing of figures

Acknowledgments

I joined QDev on the 1st of September in 2015. To everyone who helped me go through the training process I want to say Thank you.

Firstly, Charles Marcus, for inventing, running, and making the QDev a pleasant place to work. Other, current and past, people at QDev to say Thank You, are Dovydas Razmadzė, David van Zanten, Morten Madsen, Mingtang Deng, Filip Malinowski, Filip Krizek, Fabrizio Nichele, Sven Albrecht, Ferdinand Kuemmeth, Hung Nguyen, Christian Volk, Jana Darulova, Shivendra Upadhyay, Karl Petersson, Jens Nielsen, William H.P. Nielsen and Coffee Molecule. Next, current and past secretaries at QDev for making everything coordinated: Jess Martin, Maria Batista, Tina Bang, Dorthe Bjergskov, Katrin Hjorth, Kathrine Conrad, Trine Boje and Tina Nielsen.

Finally, I thank Miglė Mockevičiūtė for always supporting me, proofreading my texts and borrowing me time. I cannot wait to pay You back in the future.

0

Outline

Performing measurements at higher frequencies is beneficial due to several reasons. Firstly, they have much better sensitivity than the corresponding low frequency (DC) techniques. Moreover, they have lower $1/f$ noise levels and a high bandwidth (BW). It comes as no surprise that the control of qubits also almost always involves timescales inaccessible with the standard low frequency techniques. The idea behind this contribution is to bring the experience from the world of high frequency techniques to topological matter community and to try to investigate the possibilities of realizing the Majorana bound states based qubit in a one dimensional solid state system. This thesis is organized as follows:

- Chapter 1 introduces the theory behind the quantum information, topological states of matter and the protocol for Majorana qubit experiment;
- Chapter 2 briefly explains nanofabrication methods and the preparation for cool-down;
- Chapter 3 is dedicated to low temperature physics techniques and methods used;
- Chapter 4 explains the fast readout and acquisition technology. It describes in detail the reflectometry technique used, detection and excitation methods and high frequency equipment;
- Chapter 5 presents the experimental data and results achieved;
- Chapter 6 summarizes and discusses the experimental findings and outlines several ideas for how it can be improved.

All data presented in Chapter 6 was measured and/or analyzed by the author with the input from the supervisor and several other members of the team.

In physics, you do not have to go around making trouble for yourself - nature does it for you.

Frank Wilczek

1

Topological states (of) matter for quantum information processing

Quantum computers store and process information in a fundamentally different way compared to its classical counterparts. Whereas the classical information is stored in sets of bits, zeros and ones, the quantum computer does that with the help of the so called qubits i.e. quantum bits[1]. A qubit is a building block of a quantum computer. In principle any well defined quantum two - level system could act as a qubit but while a classical bit only has two possible states (0 and 1), the qubit can be in a superposition of those two states. Every time we add an additional qubit to our system we double the number of possible states in computational space. Mathematically qubit ability to be in a superposition of $|0\rangle$ and $|1\rangle$ is expressed as:

$$|\psi\rangle = \alpha\,|0\rangle + \beta\,|1\rangle \tag{1.1}$$

When making a measurement on a qubit, its state, instead of staying in a superposition, collapses to one of its constituents $|0\rangle$, or $|1\rangle$[1]. As a result, we get an output which is probabilistic. The probability for a particular output is given by the squared coefficients (α or β) describing the state $|\psi\rangle$. Even though the field of experimental quantum computing has seen an immense amount of progress in the last twenty years[2,3,4,5,4,6,7,8], in all of the quantum computing schemes demonstrated so far, be it superconducting, spin, charge, trapped ions or optical qubits, one of the long standing and still not overcome challenges is fighting against the decoherence. Decoherence is defined as a loss of coherent superposition of two or more states - an ingredient a quantum computer gets its power from.

1.1 Majorana fermions and Majorana bound states

The Majorana Fermions (MF) have a relatively long history in scientific literature. First predicted in 1937 by an Italian born physicist Ettore Majorana it was defined to be a charge neu-

tral, spin half particle and, what is more, to be its own antiparticle[9]. The prediction was based on Dirac's theory of an electron[10]. It was thought to occur and be realized in special types of particle collisions in space. Without much evidence from the outer space, during recent years theoretical physicists have realized that a similar form of Majorana - like excitations could effectively be realized in a solid state system in almost a table top experiment. However instead of being called MF in condensed matter, it is more precise to call it a Majorana Bound State (MBS) or Majorana Zero Mode (MZM). This is because it is only a quasi-particle version of MF that is realized in a solid state system, i.e. a solid state excitation satisfying similar commutation relations as real MFs do. Here we are interested in a solid state approach to MFs and as such we will refrain from any further discussion about MFs in space. However, an interested reader is referred to[11,12,13,14,15]. Proceeding with the theoretical description of MF, here we introduce what we call the Majorana creation $\gamma_i^\dagger$ and annihilation γ_i operators. They satisfy the condition:

$$\gamma_i^\dagger = \gamma_i \tag{1.2}$$

This condition is a direct reflection of the definition that MF is a particle which is its own antiparticle.

Quantum mechanically the behavior of a particle is described by its wave-function (WF). In physics there are two well known types of particles having different statistics: bosons (WF gets a "+" sign under exchange) and fermions (WF gets a "-" sign under exchange). It turns out that the MZMs satisfy yet another set of rules when particles are exchanged. Particle statistics is said to have a non - Abelian nature, i.e. the order in which the particles are moved around each other matter and the WF gets multiplied by a matrix instead of just a scalar. The product of two matrices is not always commuting, hence the name non - Abelian. Some-

times MZM is said to encode "half an electron" degree of freedom and, as such, two MZMs would be needed to represent the presence or absence of a single electron. Mathematically this would mean that the creation $\gamma_i^\dagger$ (or the annihilation due to particle being its own antiparticle) operator can be written as a sum of the creation and the annihilation operators of an electron. $2N$ MZMs encode 2^N degenerate states (2^{N-1} if the parity is conserved). Exchanging a certain pair of MZMs among the $2N$ available would be equivalent to a rotation (matrix multiplication of the quantum state) of the system. Multiple such exchanges would work as an equivalent of quantum gates. The striking thing is that if one could imagine being able to control MZMs independently and somehow separate them by large distances, one would still have a well defined parity state of MZM being occupied with a single electron or not. The non - locality of MZMs also means a high degree of natural protection of the encoded quantum information against decoherence. As long as the parity stays the same - the state would be protected. In order to destroy the state one would have to act on both "sides" simultaneously which is much less likely when the MZMs are separated.

1.2 Kitaev's model

About 15 years ago a Russian mathematical physicist Alexei Kitaev came up with a theoretical model for engineering MZMs in the condensed matter system. In his model MZMs appear as end states in a 1-D system (superconducting nanowire) made out of a p - wave superconductor (SC). In p - wave SC the electrons pair with a finite momentum rather than with 0 momentum as in conventional s - wave SC[16,17]. The Kitaev's model goes as following: it is a one-dimensional chain with N sites, exactly like in the well known Hubbard model. Each site in the chain can be occupied by an electron. However what is absent in the Hubbard's

model is superconductivity and this is exactly what Kitaev added. In terms of the Majorana operators (MO) and under several simplifying assumptions a typical model Hamiltonian for a Kitaev chain can be written as:

$$\mathcal{H}''_{chain} = it\sum_{i}^{N}\gamma_{i,2}\gamma_{i+1,1} = 2t\sum_{i}^{N-1}\tilde{c}_i^{\dagger}\tilde{c}_i \tag{1.3}$$

What is interesting is that the Hamiltonian does not involve two end MZMs. As a result, they commute with the Hamiltonian. What Kitaev discovered was that while in the trivial regime in a one dimensional chain MO from the same site tend to combine into a single fermion, in the topologically non - trivial case, as in the Hamiltonian above, the MO from adjacent sites form a fermion thus leaving the two unpaired MO at the two opposite ends of the chain living at zero energy. Thus, to sum up MZMs appear at the ends of a 1-D p - wave SC.

1.3 Is it possible to avoid P - wave superconductor?

Theoretically, several solid state systems have been proposed as potential candidates for showing MZMs[18,19,20,21,22,23,24,25]. Almost all proposals up to now incorporate a state of matter known as a topological superconductor (TS). The Nobel Prize in Physics in 2016 was awarded for work on TS and topological states of matter. A TS is a material that has a superconducting gap in the bulk but shows protected (metallic - like) states on its boundaries. This means that the surface of TS contains conducting states and electrons can only move along the surface of the material. TS can be realized in one (1-D), two (2-D) or three (3-D) dimensions but here we limit ourselves to 1-D case only as it is simplest to understand and is more relevant to studies presented here. The problem with all previous proposals, including the one from

Kitaev is that they all require having as already mentioned above p - wave superconductor where electrons pair in a triplet state as opposed to an s - wave singlet pairing. Whereas the singlet pairing is preferred in most known SC, so far, no or very few robust p - wave superconductors are available for condensed matter experiments. In order to bypass this problem and to realize a system that could potentially have MZMs, several ingredients were outlined in a milestone paper in 2008 [26]. In a 1-D semiconducting (SmC) wire those ingredients are:

- strong spin - orbit coupling (SO);
- conventional s - wave SC induced in the wire;
- magnetic field applied perpendicular to SO axis;
- large g - factor in the SmC.

If all the requirements are satisfied in the 1-D system it effectively shows signatures of the p - wave superconductivity, which is exactly what is needed to realize MZMs and open the so called topological gap protecting MZMs given by:

$$E_{Gap} = \left| E_Z - \sqrt{\Delta^2 + \mu^2} \right| \tag{1.4}$$

where Δ is the proximity induced superconducting gap, μ is the chemical potential usually tuned by gates nearby the nanowire (NW), and B is the magnetic field applied along the NW axis. The first signatures of the experimental data consistent with the interpretation as MZMs as proposed by Oreg et al. and Lutchyn et al. were reported in [27] and reconfirmed by several other groups soon after [28,29,30].

1.4 Quantum computing in one dimension

This work tries to explore the first steps towards MZMs based quantum information processing (QIP), namely Majorana qubit with an approach outlined by Aasen et al.[31]. The procedure is based on a SC - SmC approach to manipulate MBS using electric gates only in a 1-D system where the magnetic field is applied along the NW axis. All characterization and control protocols involve only low and/or high frequency measurements. In Majorana based QIP the milestone experiments that one could aim to demonstrate before fully exploiting the MZMs for QIP purposes as outlined in[31] are:

- braiding - demonstrating the underlying non - Abelian statistics of MZMs in triple junction networks that would allow the exchange of MZMs;
- fusion rule - demonstrating probabilistic 50:50 output when merging two MZMs, indicating that the electron mode composed out of two MZMs is either empty or occupied;
- Majorana qubit - measuring the relaxation - T_1 and coherence - T_2 times.

Here I will only be concerned with the first steps towards the Majorana qubit experiment.

1.5 Parity - to - Charge conversion

Before the exact procedure on how to perform the Majorana qubit manipulation are introduced let us outline the "parity - to - charge conversion" protocol (Figure 1.1). In our case, the experimental system is a SmC InAs/Al NW (gray) which is coated with a SC Al shell (red). The lead (blue) is a bulk Sc usually same material as red but not necessarily. In between the

lead and the main island there is a gate controllable barrier that allows changing the tunnel rates for electrons.

For the qubit experiment it is of utmost importance to be able to control the ratio of the Josephson energy (E_J) and the charging energy (E_C) of the island since this is the most important parameter in order to avoid the residual E_C dominant MZMs overlap. When the island, via E_J[32], couples to the lead much more strongly than the E_C of the island (a typical situation when the barrier is open, black, also known as a "cutter"), the even and the odd parity states are degenerate. Here we assume that the island is tuned into such a regime that two MBSs appear at the two ends of the SC island (Figure 1.1a), adapted from[31] and was used before in[33]. The other gate (blue) known as a "plunger" V_g changes the carrier density μ in the island region and alleviates the transition to the topological regime. After closing the cutter, the E_C starts dominating and the even and the odd parity states are split (Figure 1.1b). As a result, two charge states appear are now well defined whereas MBSs disappear. This is exactly what is known as a parity - to - charge conversion - going from the E_J dominated regime to the E_C dominated regime.

Both, in the parity-to-charge conversion protocol, as well as in the Majorana qubit protocol in the E_J dominated regime, it is important to not accidentally change the parity state during the readout or manipulation, for example by quasi-particle (QP) poisoning. Hence, it becomes important to have the leads longer than the characteristic coherence length associated with the SC so that parity still has a chance of being conserved even if the poisoning event happens.

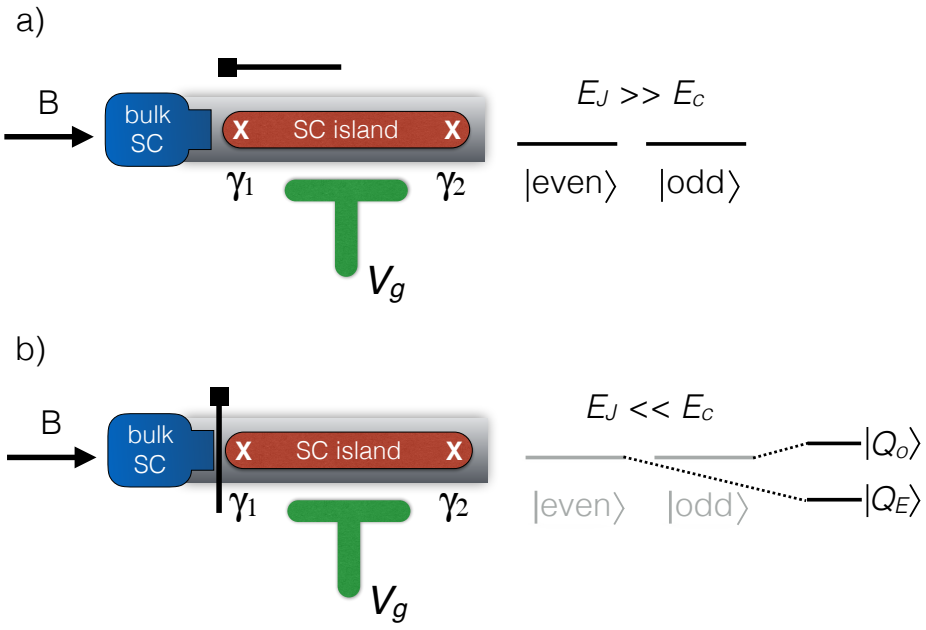

Figure 1.1: Parity - to - charge conversion. Image shows a semiconducting nanowire (gray) which is coated with superconducting shell (red). The lead (blue) is a bulk superconductor. In between the lead and the main island there is a gate controllable barrier that allows changing the tunnel barrier between the two islands. By operating the barrier voltage as outlined in[31] this configuration allows Majorana zero modes parity-to-charge conversion. Figure adapted from[31] and was used before in[33].

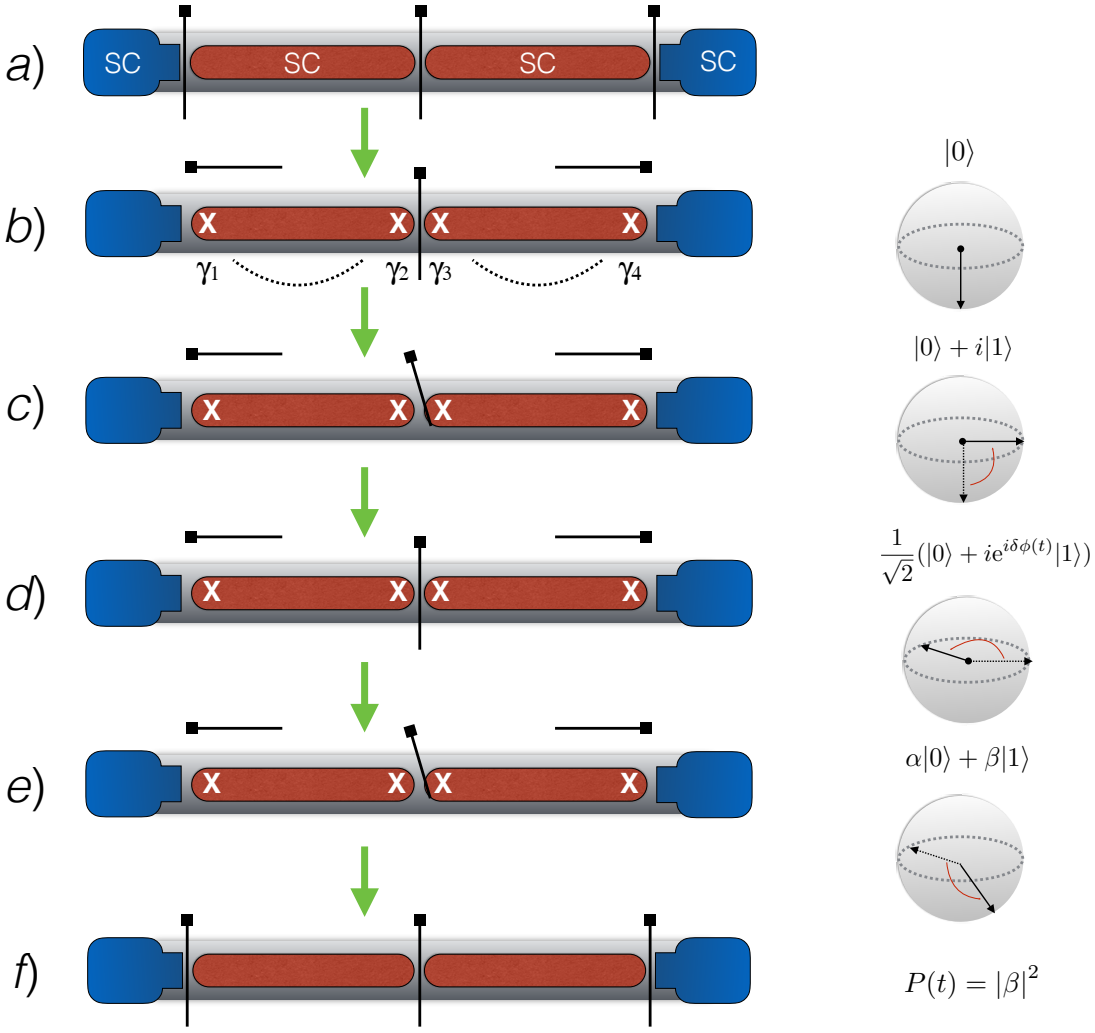

Figure 1.2: Majorana qubit protocol for measuring the coherent oscillations[31]. Going from top to bottom a) Initialization of double dot, b) initialization of qubit, c) apply $\pi/2$ pulse, d) unitary evolution for time t, e) apply another $\pi/2$ pulse, f) readout. Figure adapted from[31] and was used before in[33].

1.6 Majorana qubit

The rotations on a Bloch sphere are decided upon the unique properties of MZMs. The left side of the Figure 1.2 (already reported in [33]) illustrates the cutter gates manipulations and the right side shows the corresponding Bloch sphere picture as adapted from [31,33]. The qubit is initialized when all the cutters are closed and the E_C is the dominant energy scale. Then the parity states are fully split. As a second step we open the outer cutters to the leads and four MZMs are synthesized. By applying the $\pi/2$ pulse, which means opening the middle cutter by some amplitude and some duration and then closing it, one implements the $\pi/2$ rotation towards the equator. The voltage pulse height is given by the two middle MZMs dominated overlap. Then, given that there is a residual E_C on the island, it drives the qubit rotation on an equator for some time until the other $\pi/2$ implements projection to the north or the south pole. Based on for how long one lets the system evolve in - between the two $\pi/2$ pulses, the coherent oscillations of the qubit's state can be obtained and T_2 time can be extracted.

Today's scientists have substituted mathematics for experiments, and they wander off through equation after equation, and eventually build a structure which has no relation to reality.

Nikola Tesla

2

Fabrication and preparation for cool-down

One of the objectives of this work was to do low - temperature (LT) measurements on the NW devices. Even though the fabrication when looking at scanning electron micrograph (SEM) might not look overcomplicated, in reality when fabricating devices one has to pay special attention to details, as even the smallest mistake, an error or a previous procedure that is not followed 100% might very quickly lead to an exponential number of possibilities why devices do not work as expected. The field of MZMs received a huge boost when Krogstrup et al.[34], with the help of molecular beam epitaxy (MBE) was able make a perfect epitaxial interface between the SC (Al) and the SmC (InAs) NW. The perfectly matched interface between two materials gives much better quality of the proximity effect, which can be seen in tunneling experiments with a typical good proximity effect signature being a hard induced SC gap as reported for the first time in[35] that is a fundamental requirement for topological quantum information processing[36,37].

2.1 Manipulating nanowires

Having the blank chips ready, the NW transfer onto a chip from the NW substrate is accomplished with the help of a micro - manipulator. One can also choose what is known as a dry or wet deposition but those are a bit outdated, as micro - manipulator technique offers the highest flexibility and selectivity in terms of positioning the NWs.

2.2 Exposing, etching aluminum and scanning electron microscopy

Given that the resist has been successfully spun onto the chip one has to expose the chip with the electron beam lithography (EBL) system. In order to have a tunnel barrier, it is needed to selectively remove the SC Al shell from the NW. Then the gold contacts and the gates can

be fabricated. Removal of the Al shell is important, as otherwise a screening will make gating hard because the current will go through the SC Al shell and not the SmC InAs/Al NW.

2.3 Metal deposition, atomic layer deposition and liftoff

The metal is evaporated and ion milling are done in a single chamber with a high vacuum. This is advantageous because in this way the sample does not have to be exposed to oxygen during the milling step or during the repeated metal deposition. Having exposed it to oxygen would be detrimental as it would create an oxide layer preventing to make good quality ohmic contacts. Afterwards the lift - off of metal follows with the help of NMP. It dissolves the resist after the metal deposition and in this case it removes the resist together with the metal on top. The previous steps including multiple EBL sessions need to be repeated multiple times separately for etching windows, ohmic contacts, atomic layer deposition (ALD) windows and gates. It is important to note that the current generation of devices have all their gates on top of ALD layer that covers part of the chip. Higher dielectric constant material (hafnium oxide - HfO_2) was used in order to reduce the voltage range needed for the cutter gates when going from E_C to E_J dominated regimes.

2.4 Gluing and bonding

To glue a chip onto a chip carrier silver paint was used. To confirm that a chip is glued successfully one can try to move or shake the chip with a tweezer, without damaging the chip. If it is glued properly one can prepare for bonding the chip to a daughter - board (DGHTB). When bonding it is important to keep both the chip and yourself grounded at all times. It is also recommended to make a fence bonding first, i.e. to short all the pads that are to be

bonded together first and only then start bonding DGHTB pads to a chip. In that case the probability of an accidental blowup of the device is minimized. In the end, if everything works out fine, one can arrive at something like shown in Figure 2.1. When bonding one has to be careful and follow relatively strict guidelines to minimize parasitic capacitance which might be very detrimental when performing fast measurements where high frequency (HF) radiation is involved:

- use helper pads only for low frequency (LF) lines (helper pads can be cut into two using a razor blade);
- keep bonding wires of fast gates and radio frequency (RF) sensing bonds as short as possible;
- avoid running them in parallel to other bonds or crossing other bonds to reduce mutual capacitance;
- remove all central fuzz buttons unless you want a cold grounded cavity.

2.5 Loading, pumping and cooling down

After bonding it is possible to put the DGHTB onto an interposer which itself sits onto the mother - board (MTHB). The MTHB sits inside of the puck, a brass cylinder which later goes into the load - lock. The load - lock itself is attached below the fridge to allow for bottom loading. Before loading it is important to remove all air from the load - lock and/or any other residues such as dust etc. The pumping usually takes up to 10 hours but sometimes much shorter periods are allowed of the order of few tens of minutes. Continuing about

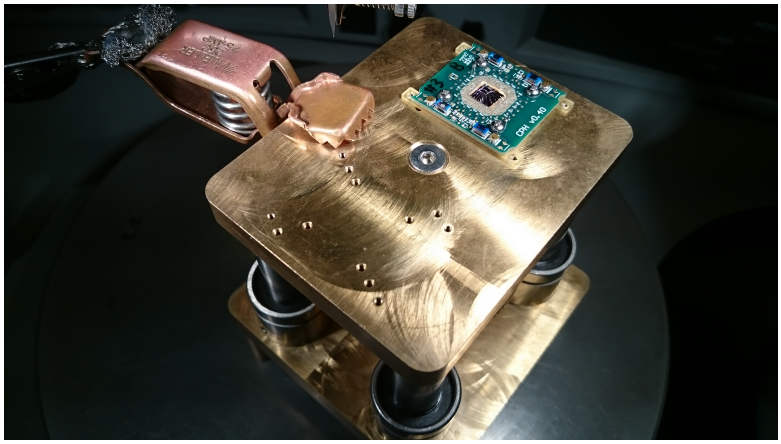

Figure 2.1: Preparation for bonding. When bonding one has to be careful and follow relatively strict guidelines to minimize parasitic capacitance which might be very detrimental when performing fast measurements where high frequency radiation is involved.

the parasitic capacitances: one of such capacitances is a capacitance to the backgate (BG). Parasitic capacitance to BG is bad because every capacitor acts as an RF ground and radiation goes towards that RF ground rather than hits the tank circuit (TC) and gets reflected. BG is in principle known to help a lot when tuning into the MZMs regime when side gates are not strong or effective enough to deplete the wire. Hence in this case we decided at least instead of using a global BG covering the full cavity area of the DGHTB where the chip is glued, as was done until now, to move to a local much smaller BG on a chip. What is more, if the contact pads go directly on the silicon (Si), there should be some static protection as the Si is leaky at room temperature but freezes out when cold. From the data acquired and tests made (not reported here) we got a rather huge improvement in the bandwidth (BW) of RF radiation reaching the sample: from about 600 MHz with the global BG to about 10 GHz with a local BG. However since the shift to local BG happened only towards the end of this thesis almost all the data presented here will be from the devices measured with the global BG present.

Measure what can be measured, and make measurable what cannot be measured.

Galileo Galilei

3

Experimental techniques at low temperatures

In recent years LT techniques gained a lot of attention due to the immense possibilities that LT measurements provide when studying quantum effects. In this chapter I tried to collect the knowledge gained during the time of this thesis as well as some insights that could help for the future generation of physicists trying to start their path in LT research.

3.1 Pulse tube cooler and dilution refrigerator

At its heart the cryostat uses a two - stage Pulse Tube Cooler. By expanding and contracting helium gas (He) it is able to effectively remove heat. The cooling action starts with the mixture which consists of He_4 and a much smaller quantity of He_3. When cooled below 0.87 K the mixture separates into two: the He_3 rich phase floating on top of the diluted phase with almost pure He_4. For thermodynamical and quantum mechanical reasons there is still about 6% He_3 left in the pure phase. The concentration of He_3 in the dilute phase can be reduced by pumping on it (transporting He_3 to the still at 0.7 K). By pumping mostly only He_3 is transported because at 0.7 K the vapor pressure of He_3 is higher than of He_4. The gas mixture that returns at higher than 0.7 K is condensed back into liquid with the help of the impedance. The impedance pressurizes the gas for it to condense at about 1.5 K. With the help of the heat exchangers the evaporating He_3 at the still cools down the mixture, which returns towards the mixing chamber. This cycle repeats over and over again and allows the mixture continuously circulate. Circulating mixture provides cooling power to the sample thermally linked to the mixing chamber. QDev dilution refrigerators have vector magnets, usually with 1 T in the x and y directions and 6 T in the z direction. The direction of the z axis field is parallel to the long axis of the puck.

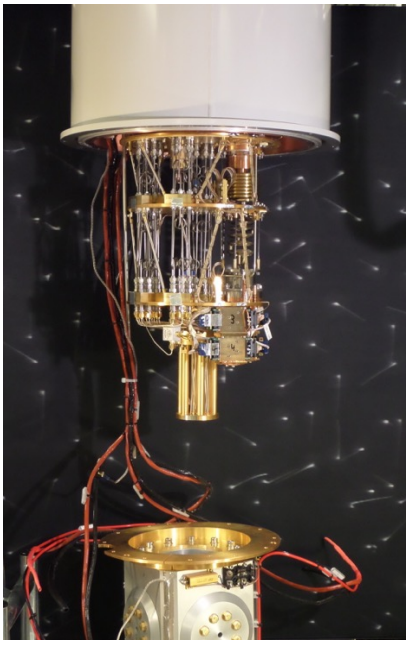

Figure 3.1: Inside view of the cryo - free dilution refrigerator at QDev.

3.2 Wiring at low temperatures

When performing LT experiments different types of wiring are used. Two main classes are LF wiring at both room and LT and HF wiring at LT. LF wiring is mostly unshielded (used for measurements at kHz frequencies and below) and coaxial cables are shielded (used for measurements at MHz frequencies). When wiring a fridge, the following set of "rules" should be satisfied:

- it is important to have good thermal isolation between each refrigerator stage going from top to bottom;
- the thermal link between the mixing chamber (MC) plate and the sample holder sitting inside the puck is of utmost importance;

- one has to keep the external radiation to a bare minimum as otherwise it might penetrate the sample and give artifacts to the measured data;
- unless it is necessary to thermalize electrons etc, any unintentional signal attenuation must be avoided since otherwise the level of signals that reach the sample might be different than expected;
- shielding the sample area is important in order to avoid pickup from stray fields.

Real life, however, is more complicated because many of the requirements outlined above are not necessarily in agreement with each other. If one aims for low thermal conductivity, a good choice would be, for example, stainless steel or niobium (SC). Electrons cannot contribute to heat conduction in the SC below the gap[38]. On the other hand, when maximal thermal or electrical conductivity is needed, copper is a good choice. For the coaxial links connecting the 70 K plate to the 4 K plate one could use copper instead of, for example stainless steel, because of its better transmission characteristics at HF[38]. Copper is also a much better electrical conductor than stainless steel (see[38]). However, this also means that copper has a larger conductivity of heat. For coaxial lines below 4 K, one can use NbTi lines. These are SC, i.e. they are excellent electrical conductors but at the same time poor thermal conductors. Speaking about the sample holder, the DGHTB is part of a modular structure and is connected to the MTHB with the help of an interposer. The interposer is fitted with 64 so called fuzz buttons which carry the signal of the 48 DC lines and the 16 RF lines from the DGHTB to the MTHB, as already reported and described in detail in[33].

3.3 Bias - tees, electron temperature and filtering

A bias - tee is a capacitor - inductor (sometimes resistor) set where the capacitor blocks the DC part but couples HF and inductor in ideal case passes DC but blocks HF. Each DC line has an associated cut - off frequency above which a signal is attenuated. Same applies for the high frequency lines where only signals above the cut - off are passed limited by the characteristic time of the bias - tee. At the output one gets the sum of AC + DC which can be applied to the sample. In QDev bias - tees are incorporated into the MTHB.

Due to the suppression of electron - phonon coupling at LT and sensitivity to electrical noise, the temperature of the electrons in the device under test is typically higher than the MC temperature. However, for many researchers it is the electron temperature in the signal lines as well as the electrical noise environment that is the most important, for example for the performance of qubits and other LT electronic devices. For the experiments presented in this thesis filtering is very important and helps in a threefold way:

- thermalization of electrons;
- noise elimination from the electronics and the environment;
- the minimization of QP poisoning.

3.4 Noise Reduction

In LT physics, like in any other physics experiment, one is trying to obtain as good and as clean signal as possible. Hence it is essential to reduce the noise levels in the data taken. This can be achieved by changing the integration time of the lock - in amplifier (LIA) for example.

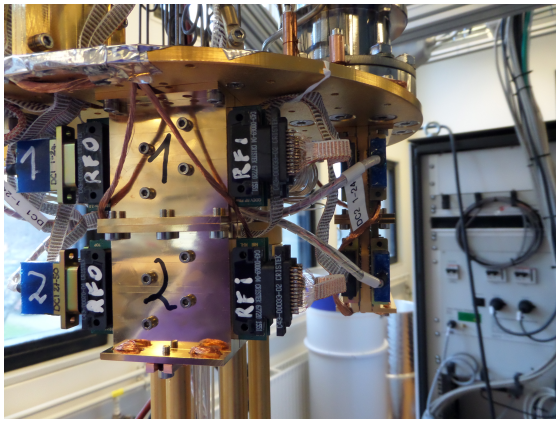

Figure 3.2: Cryogenic filters for filtering high frequency noise on low frequency lines.

Doing so will result in a quieter signal at the expense of a longer acquisition time needed. There are a few things to be aware of when setting up a measurement setup:

- keep all instruments on the same ground as the dilution refrigerator, i.e. avoid ground loops;
- do not introduce any equipment that is not needed for the experiment as this helps to minimize the number of ground loops;
- physically separate noisy equipment such as computer box, power supplies, etc, from sensitive equipment, such as LIAs.

I have done a terrible thing, I have postulated a particle that cannot be detected.

Wolfgang Pauli

4

Fast readout and manipulation: techniques for Majorana based quantum information

For many years, each of the solid state approaches to QIP showed not very different levels of promise and development with no clear leader in the horizon. This all changed when Nakamura et al. in 1999 demonstrated the first coherent control of a macroscopic quantum two - level system in a charge qubit[39]. There, one applies voltage pulses to a gate electrode, which is capacitively coupled to the superconducting Cooper pair box (CPB). It was possible to manipulate the quantum states of the island - charge qubit. Coherence between the adjacent charge states was observed, proving for the first time that it is possible to control and measure a quantum two - level system. However, coherence times observed were relatively short of the order of few nanoseconds.

4.1 Reflectometry and matching resistance

Even though the above mentioned results by Nakamura et. al were achieved when performing slow, highly averaged instead of time resolved measurements, to have ultimate control, sensitivity and resolution one has to move to fast, HF measurements. The reason for this is because in principle it allows a single shot readout of the state (readout time is shorter than T_1 time of the system). It is also known to reduce the levels of $1/f$ noise. This is due to the fact that one is working at HF, instead of measuring averaged DC current. Below, the so called reflectometry (RFL) technique as well as the fast acquisition suite used and partly developed during the time of this thesis will be detailed. Pioneered by Schoelkopf[40] and further adapted for use in spin qubit experiments by D. Reilly[41] and others[42,43,44,43,45] this method gives an effective bandwidth in the MHz range.

The first requirement to use the RFL technique for the readout of a charge sensor is the resonant resistor - inductor - capacitor (RLC) circuit in which the charge sensor is embedded.

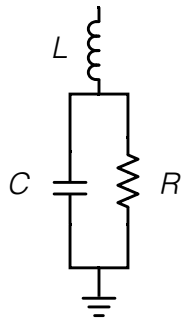

Figure 4.1: The tank circuit. Inductance *L* is provided by the surface mount inductor, capacitance *C* is the parasitic capacitance coming from the bonding wires and other mount elements and *R* is given by a charge sensor in the device.

The resonant RLC circuit at some frequency f has its impedance close to the characteristic impedance of the transmission line which is $Z_0 = 50\ \Omega$. If this condition is fulfilled, the RLC circuit is said to be impedance matched. The RFL circuit in the experiment includes four parallel resonant *RLC* (or "tank") circuits (Figure 4.1), theoretically enabling fast sensing of multiple charge sensors simultaneously. Similar tank circuit was already presented in [33].

Lets try to delve a bit deeper into the technique itself. The idea behind this method is to sense indirectly the impedance change of a quantum dot by monitoring the amplitude and/or the phase of an RF wave reflected from a quantum dot (QD). If a wave travels in a medium with an impedance Z_0 and it encounters an environment with a different impedance Z_1, the wave will get reflected back with a reflection coefficient given by:

$$\Gamma = \frac{Z_0 - Z_1}{Z_0 + Z_1} \tag{4.1}$$

It can be shown that the matching condition will be obtained when the sensor conductance (g), inductance of a surface mount inductor soldered onto the board (L) and mostly parasitic capacitance (C) coming from bonding wires, surface mount elements etc, satisfy the

following condition:

$$Z_o = \frac{gL}{C} \tag{4.2}$$

here Z_o=50 Ω. The impedance of a circuit is frequency dependent and this helps us to achieve the matching of the TC to Z_o = 50 Ω of the transmission line. Typical reflection parameter S_{21} frequency dependence from the real experiment is depicted in Figure 4.2 and in Figure 4.3. In case of perfect matching the signal sees only an RF ground while in case of a mismatch, part of the signal gets reflected. The reflected power is proportional to the mismatch. In our case, the reflected signal is measured via homodyne detection using HF lock - in techniques to be described later and also before in [33]. Experimental matching resistance can be extracted by sweeping some of the gates (or BG since then matching conditions for both sensors can be measured simultaneously) of the sensor wire i.e. changing its conductance and at the same time recording the S_{21} parameter as a function of the gate value and the frequency of the RF radiation. Experimentally it was found that the inductor that works best when both the matching condition and the range of frequency input of the demodulator are taken into account was about 4.7 μH [33] (Figure 4.4).

4.2 Homodyne detection: Ultra High Frequency Lock-In Amplifier

There are 28 high frequency SMP connectors on the cold finger. 15 of them are used for HF lines and one is the RFL line. The other 12 are not connected to anything but are terminated inside of a puck. Via a directional coupler's coupled port the signal is sent towards the sample (Figure 4.5). The amplitude of the excitation signal reaching the QD needs to be very small. This is in order not to heat up the electrons. The excitation signal is sent from the HF lock - in output port to the cryostat. The reflected signal passes through the directional coupler's

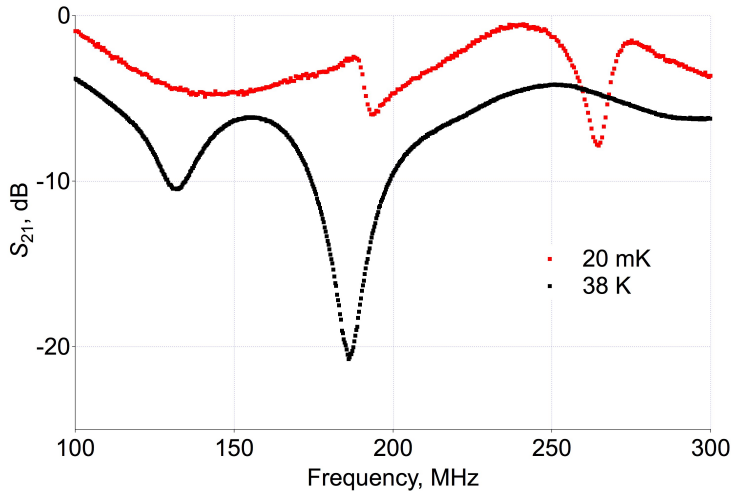

Figure 4.2: Typical application of vector network analyzer. It was noticed during the first set of experiments that the resonance frequency is temperature dependent. Shown are two graphs, black - at 38 K (mixing chamber temperature), red - at 20 mK. One can clearly see a shift of resonance frequencies towards the high side as we approach the base temperature of the dilution refrigerator.

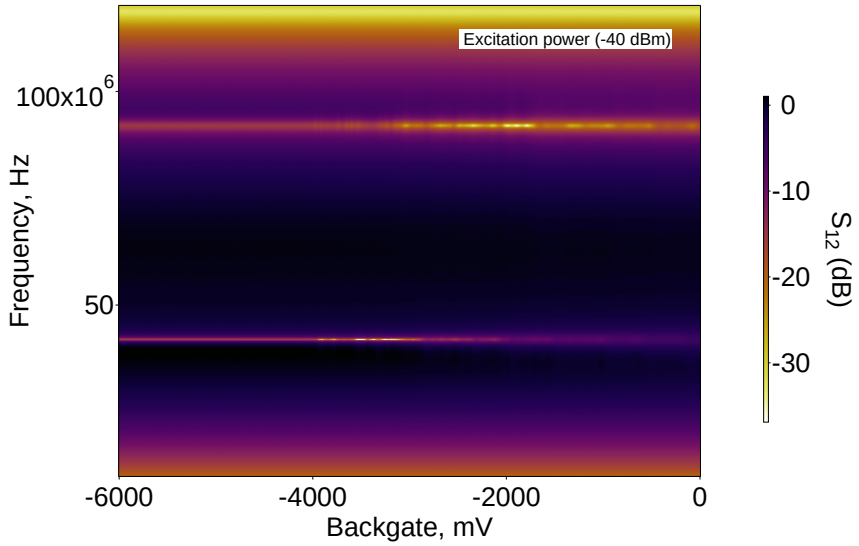

Figure 4.3: Matching condition for two sensors. When sweeping the backgate the sensor resistance changes and we go through the matching condition.

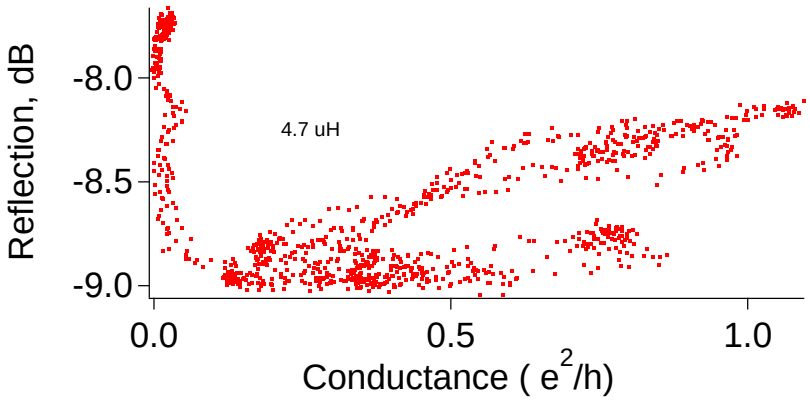

Figure 4.4: Sensor conductance versus reflection from the tank circuit (4.7 μH inductor). The matching condition (minimal reflection) happens at low conductance values.

input to output ports and gets amplified with a low noise cryogenic amplifier. The amplifier is at LT because that way their noise levels can be reduced a lot. The amplified signal is fed into the HF lock - in's input port where it is demodulated and low pass filtered.

Lock - in amplifiers are devices that allow to measure the attenuation and the phase shift of an applied signal at a specific frequency. This is useful if the signal one wants to measure is noisy because the lock - in amplifier picks out only the frequency of interest - the reference. The Zurich Instruments Ultra High Frequency Lock-In (ZI UHFLI) model can demodulate the signal and work up to 600 MHz. It generates a reference signal of a user defined amplitude and frequency, and measures the amplitude of the signal received through its input by demodulating it at that particular frequency using homodyne detection. The demodulated signal carries the information about the sample state. Before I move on, I want to mention several tips acting as guidelines that were discovered and endorsed during the thesis. It could act as a checklist for a more proper and reliable measurements when using the ZI UHFLI:

- in order to avoid the overload of the UHFLI one can set the LIA to use only half of its

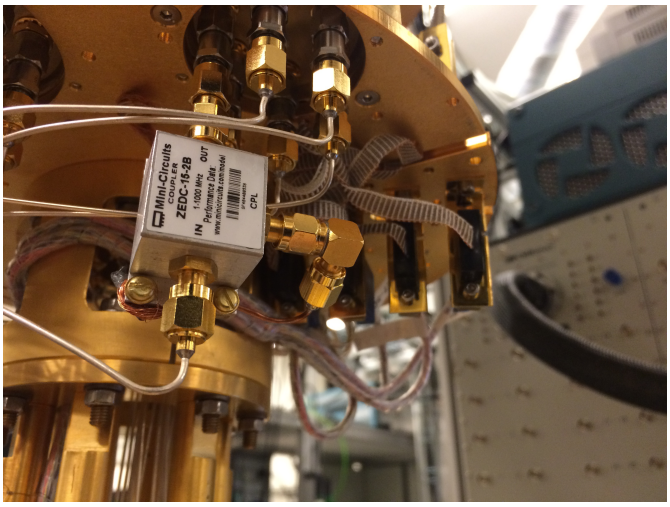

Figure 4.5: The directional coupler is a part of the reflectometry circuit mounted under the mixing chamber plate.

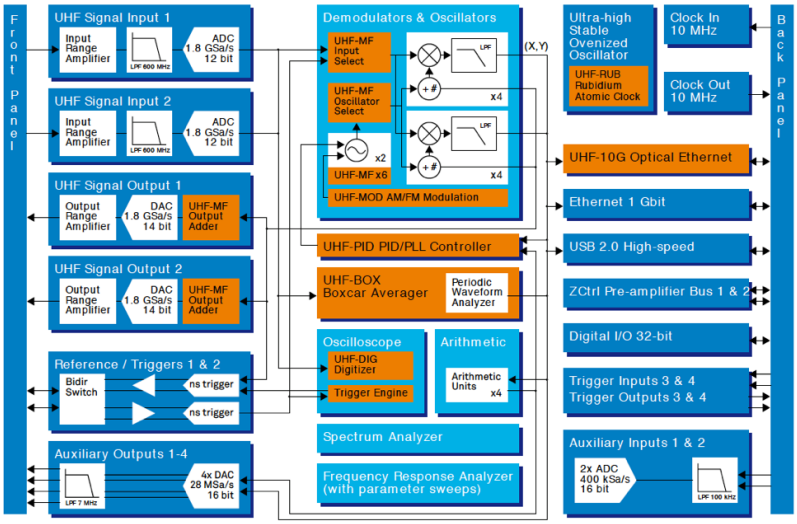

Figure 4.6: Schematic diagram of the Ultra High Frequency Lock-in amplifier internal workings. Some additional internal wiring between different components might be not shown.

input range. LIA amplifier also shows the least amount of distortions in this range;

- one can minimize the potential number of ground loops by using the internal generator of the LIA for the excitation source instead of using the external generator;

- when performing HF measurements it is important (when possible) not to use similar or the same frequencies in different equipment connected to the same setup, be it a signal generator frequency, frequencies of demodulations, trigger frequency or sampling frequency. Having similar frequencies might cause various beating effects that are hard to track and leads to unnecessary time spent when troubleshooting the setup;

- if one needs to demodulate at two different frequencies - use the LIA's capability to do exactly that. Input the signal on one of the inputs at both frequencies instead of splitting the signal with a power splitter and then using both inputs. In this case, one does not reduce the signal to noise ratio before entering the input of an amplifier. Having an additional power splitter outside the LIA would degrade the signal more than when the splitter is absent.

4.3 Arbitrary waveform generators and RF switches

Arbitrary waveform generator (AWG) can generate user defined advanced waveforms. The AWG used in the experiment was the Tektronix AWG5014. It can produce a user defined waveforms at a maximum sampling rate of 1.2 GS/s. It also allows advanced sequence control. When applying the pulse it is advantageous to have the average voltage over a single period of pulse as 0. This is because otherwise the DC voltage will drop across the bias tees in a sample board and might introduce unnecessary heating.

4.4 Synchronization

When performing HF measurements it is important to have all HF equipment synchronized to the same time base reference. Otherwise what might happen over sufficiently long times is there might be a frequency or phase shift between two or more signals. To avoid synchronization issues the setup was equipped with the rubidium 10 MHz reference. It acted as a master clock source and all other instruments having 10 MHz reference input were connected to it with the same cable length. Having the same cable length is also advantageous in terms of thermal expansion and contraction since it will supposedly act in the same ”direction” in all cables.

4.5 Fast charge diagrams

Fast charge measurements not only allow better sensitivity but also can speed up measurements a lot. One such implementation of RFL in lab jargon is known as ”fast charge diagrams” (FCD). To perform the measurements of FCD which typically is some 2-D gate - gate scan where the demodulated voltage is measured as a third coordinate allows to speed - up the measurements immensely by making one of the gate axis ramp fast, instead of both axis being slow as in standard LIA measurements. This is achieved by applying a sawtooth wave on one of the gates - ”fast” axis, while the other is being stepped - ”slow”. At each slow gate voltage one sawtooth period is applied (or a number of them and averaged together to increase S/N ratio) and at the same time a demodulated voltage is recorded which is plotted on a color scale. The demodulated voltages were recorded with the help of UHFLI which was triggered at the beginning of each sawtooth period with a trigger from a waveform generator.

"Slow" DC voltages were sourced from QDAC - a QDEV made digital to analog converter (DAC), hence the name QDAC, while "fast" axis was swept with the help of Agilent 33250A generator. The sawtooth was added to the corresponding channel DC voltage with the help of a bias - tee which resides on a MTBD. The frequency of the sawtooth was usually around 2.8 kHz. It is very important to keep in mind that the integration time for a single point in a fast charge diagram should be such that we wait enough time to integrate compared to 2 kHz sweep rate. This means that we probably do not want to sweep the fast axis at 100 kHz since then we would not let enough time for signal to be integrated at each point in a graph and data would look very noisy and/or smeared. The lower bound for sweeping frequency is given by the characteristic cut - off frequency of the bias tee which is around 1 ms. The full schematics and a photo of the experimental setup are shown in Figures 4.7 and 4.8 respectively.

4.6 *QCoDeS*: Data acquisition framework

QCoDeS is a Python - based data acquisition framework developed by the Copenhagen / Delft / Sydney / Microsoft quantum computing program. It is an open source software and is now more and more used at QDev. It was tested for the first time on the setup that includes the dilution refrigerator on which the author has worked on during this thesis. *QCoDeS* were designed to have the advantages from the open source software world as well as the most useful commands from the previous *Igor* acquisition suite. The goal of *QCoDeS* is a common framework for scientific experiments, controllable by a computer from anywhere in the world with many degrees of freedom. As developers of *QCoDeS* say, "it will enable scientists to get started more quickly in experiments, equips them with the knowledge they need to move smoothly across labs and teams, and facilitates easy writing of custom extensions". About

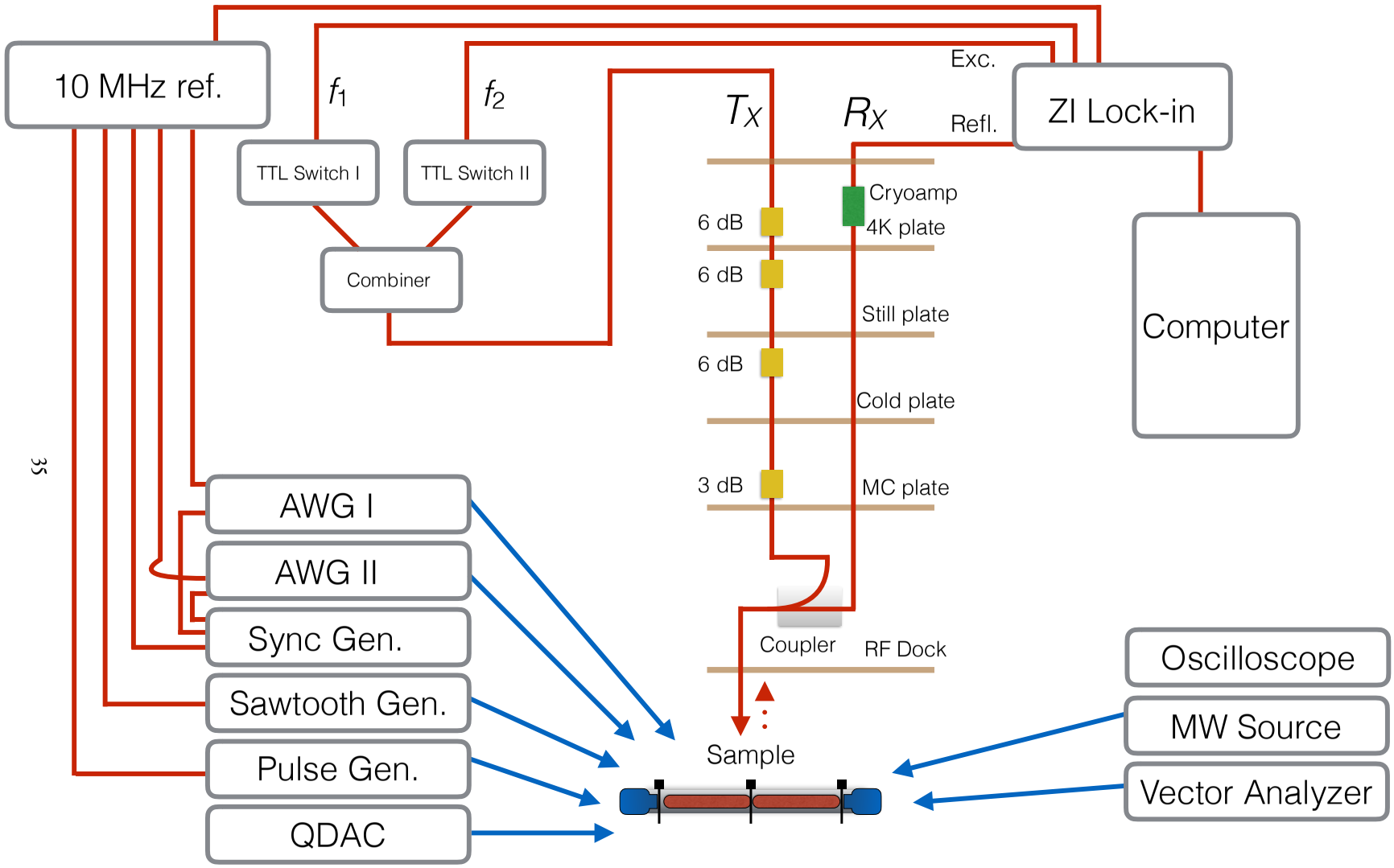

Figure 4.7: Fast data acquisition setup.

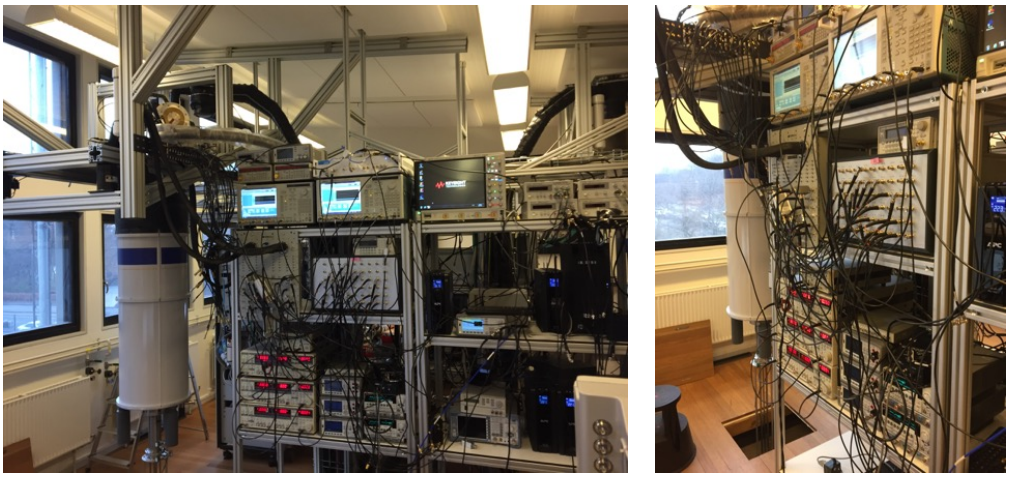

Figure 4.8: The data acquisition setup.

half of the data shown in this thesis was acquired using the *QCoDeS* suite.

An experiment is a question which science poses to Nature
and a measurement is the recording of Nature's answer.

Max Planck

5

Charge makes sense: controlling superconductor-semiconductor quantum dots

The basic characteristics defining the SC is its diamagnetic behavior, dissipation - less current and the energy gap. i.e the ground state of the SC where the Cooper pairs form. The Cooper pairs live at Fermi energy and are below the unpaired QP living outside the SC gap. The superconducting gap of the SC is usually denoted as Δ and for Al is approximately 180 μ eV. This energy gap structure can be probed by the tunneling spectroscopy briefly explained below. All measurement presented in this thesis were carried out in a dilution refrigerator with a base temperature of about 10 mK - 15 mK, configured for HF gating, LF transport measurements as well as RF RFL based readout studies. When performing LF measurements the conductances were obtained using 8 μ V - 10 μ V excitation voltages at around 133 Hz and sometimes at 77 Hz. Time constant was chosen to be 30 μ in almost in all cases.

5.1 Superconductor-semiconductor quantum dots

QD also known as an "artificial atom" is a structure that has a discrete energy spectrum. The discrete nature of the spectrum reveals itself only by the time the dimensions of the QD become smaller than some characteristic length scale. Here we will report the results achieved in characterizing the superconductor - semiconductor hybrid QD in quasi-1-D dimensional NW systems similar to some reported before[46,33]. Here it is worth to mention that the more proper term for the system investigated here would be "islands" instead of QD because by definition the QD is an object that shows the energy level quantization. In the measured devices we are unable to see the level quantization defined physics but only the charging energy effects. However where it does not cause confusion I will use the term island and QD interchangeably. In practice QD are just electrostatically confined part of material, for example by applying negative voltages at two points along the 1-D SmC NW - single QD, or at three

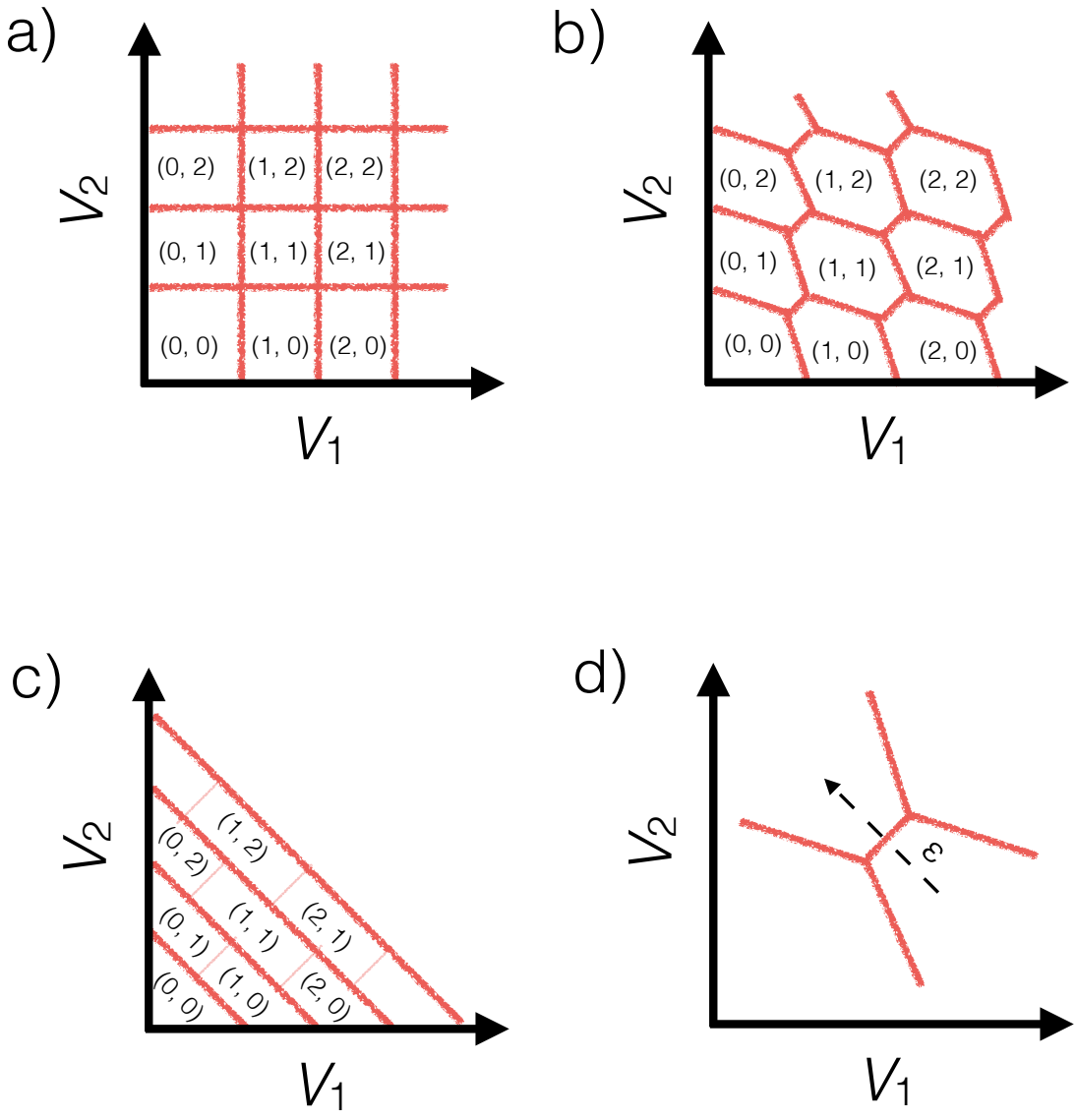

Figure 5.1: Stability diagram of the double dot system: a) small inter - dot coupling, b) intermediate inter - dot coupling, c) strong coupling - single dot regime, d) zoomed - in triple points in intermediate coupling regime.

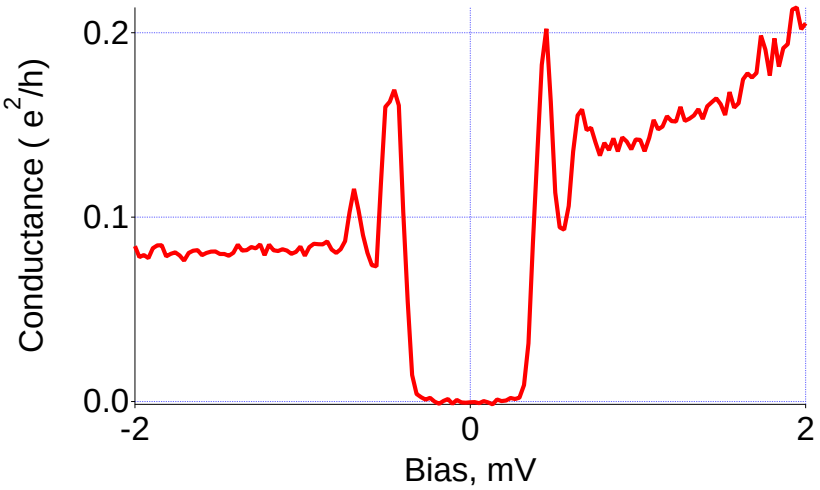

Figure 5.2: Conductance measurement as a probe for density of states.

points along the 1-D SmC NW - double QD (DQD). Negative gate voltages create tunnel barriers for the electrons and in that way confine them between two or three barriers. From the electrochemical potentials of the QD one can construct a charge stability diagram giving the equilibrium electron numbers N_1 and N_2 as a function of the two plunger gates (Figure 5.1) controlling the electron number on the two superconducting islands QD. The numbers in parenthesis show the occupation of the left and the right dot respectively.

5.2 Tunneling spectroscopy

The advantage of tunneling spectroscopy as described in [47] by Blonder, Tinkham and Klapwijk and in [48] is that in the tunneling regime ($g \ll e^2/h$, e^2/h is the conductance quantum) it can reveal and is proportional to the density of states (DOS) of the system. In more mathematical terms that means that the differential conductance measured at the bias voltage V_{SD} is proportional to the density of states in the superconductor at energy E=eV_{SD}. Figure 5.2

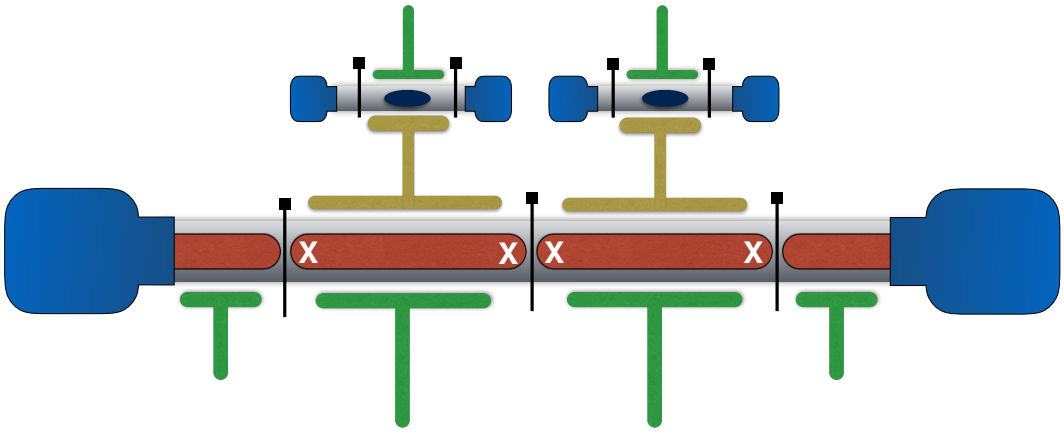

Figure 5.3: Design drawing of the Majorana qubit. Grey is InAs nanowire, red - un-etched Al, blue - golden leads, green - plunger gates controlling the electron density in the wire and tuning the Coulomb oscillations in a "quantum dot" regime, black - cutter gates forming tunnel barriers, yellow - capacitive coupler between the two islands - the main island and the sensor island.

shows a similar to Blonder-Tinkham-Klapwijk (BCS) density of states of in InAs/Al NW induced superconductivity recorded by sweeping the bias of the NW and recording the differential conductance as a function of bias. The geometry of the device was as close as possible to a normal metal - insulator - superconductor (N - I - S). In the QD regime the conductance in the tunneling regime is not necessarily proportional to the DOS of the *S* part but instead reveal some convolution of DOS of several superconductors. However it is usually still used as an indication of whether one is in the tunneling regime with the barriers defining the QD or not.

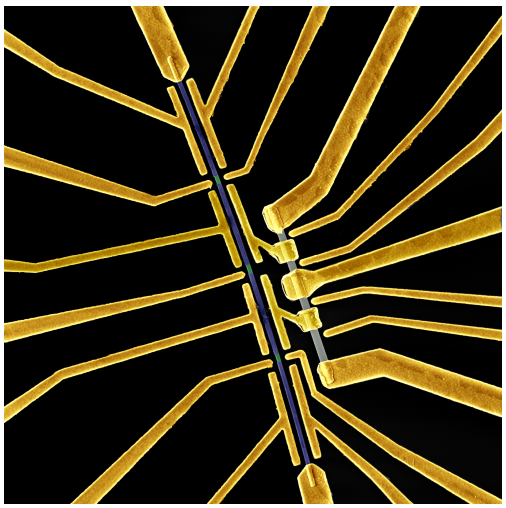

Figure 5.4: Scanning electron micrograph of the lithographically identical device measured in this work (courtesy of D. Razmadzė).

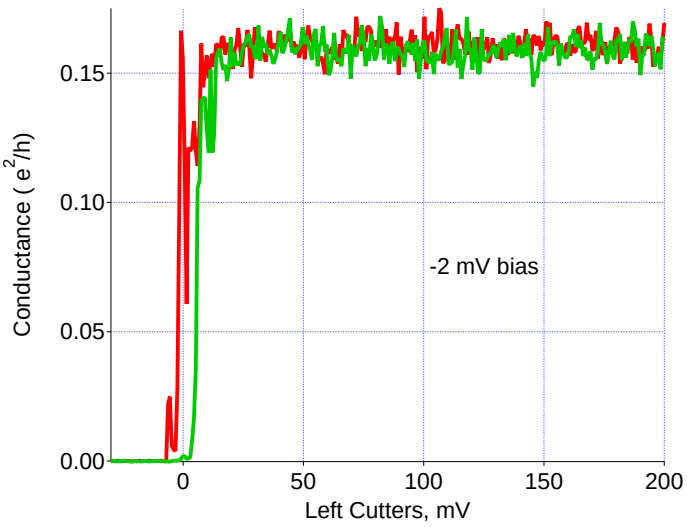

Figure 5.5: Pinch - off curve in the device with the gate dielectric for the left cutter as an example (red and green corresponds to forward and backward sweep respectively). Pinch - off curves are much more sharper with gate dielectric layer than they are without it due to high dielectric constant of the dielectric.

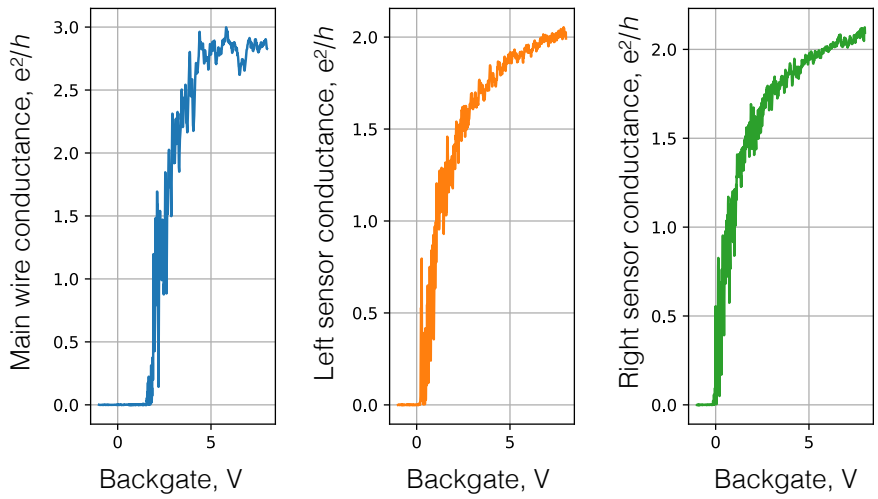

Figure 5.6: Pinch - off curves for the main wire and sensors taken simultaneously when sweeping the backgate. The almost identical pinch - off values and the shape of the two sensors (orange and green) indicate that the sensors can be made nearly identical with the most probably very similar sensing capabilities.

5.3 Control of superconducting islands

The design drawing of the typical device geometry that could potentially act as a MZMs based qubit is shown in the Figure 5.3. Grey is InAs NW, red - un-etched Al, blue - golden leads, green - plunger gates controlling the electron density in the NW and tuning the Coulomb oscillations in a QD regime, black - cutter gates forming tunnel barriers, yellow - capacitive coupler between the two islands - the main island and the sensor island. The finished fabricated device is shown in Figure 5.4. Almost all data (apart from where it is mentioned otherwise) presented in this work was measured on devices lithographically very similar to the one shown in Figure 5.4. The device has two superconducting islands and two tunable QDs. What is shown is a long InAs/Al NW with epitaxial few - facet Al where Al is etched away in places where tunnel gates are. Wider gates in between the tunneling rates controlling gates

are known as "plungers". Plungers are used to tune the density of carriers μ in the superconducting island. MZMs appear at the end points of the superconducting island.

CB regime is defined to be the regime of $E_C \gg k_B T$ where E_C is a charging energy of the QD. E_C can be imagined as the energy cost to add an additional electron onto a QD and is given by e^2/C_Σ. Here C_Σ is the total capacitance of the QD. It includes contributions from the source and the drain as well as capacitance to any other gates nearby. In a CB regime the electron number N is well defined. The device is designed in such a way that each superconducting island has its own sensor QD laying nearby and is supposed to sense the main island charge when it is in the CB regime. The sensor is nothing but another InAs NW but this time shorter and with no aluminum on it. The sensing mechanism will be detailed later in this chapter. The leads of the main NW are made effectively superconducting by making their length longer than QP coherence length. The tunnel gates control the ratio of E_J to charging energy E_C of the island. In the regime where $E_J > E_C$ the number of electrons on either of the superconducting islands formed is not well defined, whereas superconducting phase φ is well defined. In the other regime where $E_J < E_C$ the opposite is true.

High bias pinch - off curves with respect to the left cutter (similar for the middle and the right cutter) as well as BG are shown in Figure 5.5. Pinch - off curves are much more sharper with gate dielectric layer than they are without (not shown). It is due to high dielectric constant of the dielectric. The very sharp pinch - off in gate space is exactly as experimentally preferred for the precise E_C and E_J dominated regimes control because commercial AWGs used in a lab can only output up to ten volts peak - to - peak amplitude which would later be attenuated by at least 21 dB. In this way if the pinch - off range would be more than 1 V or 2 V and it might be troublesome to apply a nanosecond resolution pulses of tens of volts

amplitude and save all their temporal characteristics before they reach the sample. Pinch - off curves for the main wire and sensors taken simultaneously when sweeping the BG are shown in Figure 5.6. The almost identical pinch - off values and shape of the two sensors (orange and green) indicate that the sensors can be made identical with most probably identical sensing capabilities. Let us note here that the pinch - off traces in Figure 5.5 and in Figure 5.6 were taken from a different set of otherwise lithographically similar devices.

When the device is loaded into a cryostat it is not necessarily given that the device NW axis will coincide with the highest amplitude magnetic field axis (z) in the cryostat. Here is where the vector magnet capabilities come into help. By rotating the field in the plane of the chip at fixed magnitude we can record how the rotation angle modulates the SC gap probed in N - I - S spectroscopy regime. The gap size should be smaller when the magnetic field is perpendicular to the NW and largest when the magnetic field is aligned along the NW. This helps to find the NW orientation. Typical field rotation data is shown in Figure 5.7. Once the wire direction is known the next useful test would be to position in N - I - S geometry and do bias vs axial magnetic field scan to see how hard the superconducting gap is in the system and when does the it close as is shown in Figure 5.8.

Being in CB regime and sweeping one of the plungers on one axis vs bias on the other axis one would see classical Coulomb diamond features as shown in Figure 5.6. Coulomb diamond graph is the most reliable way to extract the charging energy of the QD. However, in this particular case it is a bit different from classical picture since diamonds are "gapped" due the gap of the SC aluminum present in the system. Inside the gap at 0 bias a 2e periodic structure can be seen. It is most probably due to the remnant super - current left after closing the barriers up to the level that the transport is still allowed but at the same time some E_C is

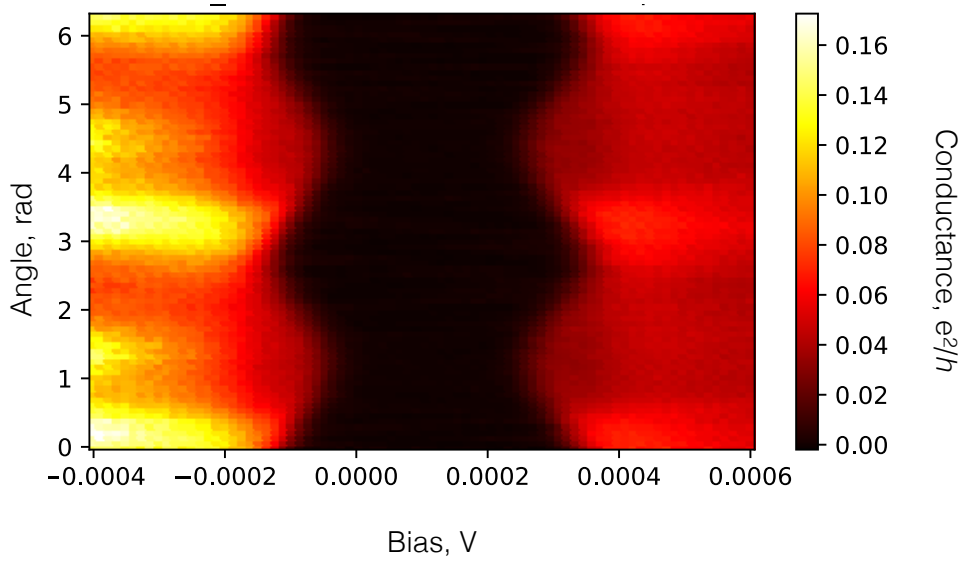

Figure 5.7: Magnetic field rotation in the plane of the sample. When the field is aligned with the nanowire axis the gap is expected to be larger compared to when the field is aligned perpendicular to the nanowire. This helps to determine the nanowire direction with respect to the axis of the magnet.

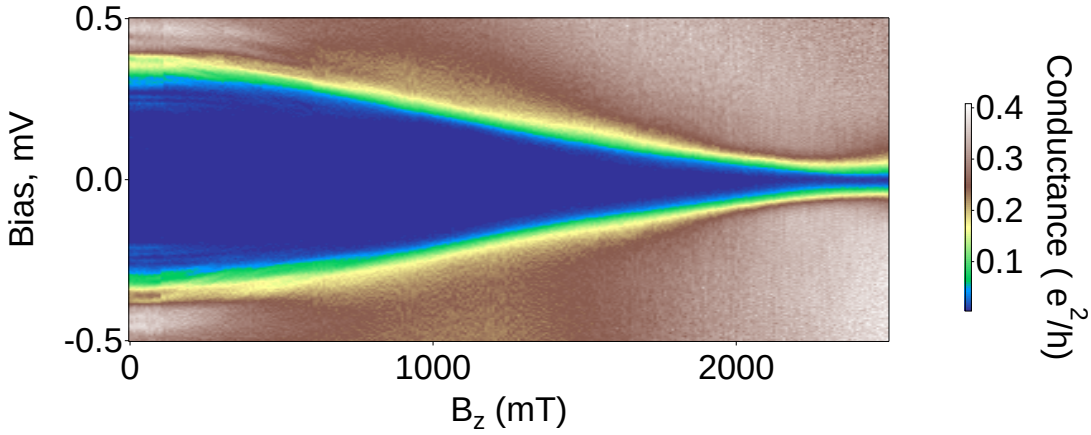

Figure 5.8: Magnetic field evolution of the superconducting gap of the system.

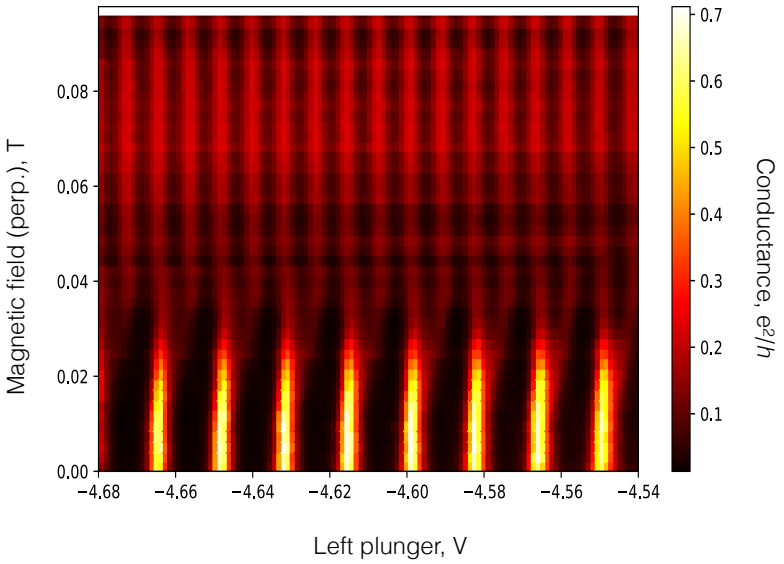

Figure 5.9: 2e periodic transport features transition to 1e periodic transport. Magnetic field effectively quenches the superconducting gap and whereas at low field transport is dominated by Cooper pairs, at higher field it is dominated by single electrons.

introduced. Similar findings were already reported in [33]. Above the gap 1e transport features are seen. This indicates the single electron transport. If we now form a DQD by partially closing all three cutters we arrive at the very similar behavior to the one depicted in Figure 5.1 d where the triple points are shown (Figure 5.11). It is almost fully decoupled DQD. The merged triple points indicate that the capacitive coupling between the two dots is almost negligible. Going more positive on the middle cutter we would successively pass through the different subgraphs shown in Figure 5.1 a, b and c.

When in single QD regime we also performed the current biased measurement. This is easy to do if the device has two split leads on each side of the wire. After performing the measurement it was possible to obtain a behavior as shown in Figure 5.12. Current biased measurement is a simple modification of a voltage bias measurement. One just needs to add a resistor (10 M"Ωin our case) of large value in series with a voltage source and use four probe

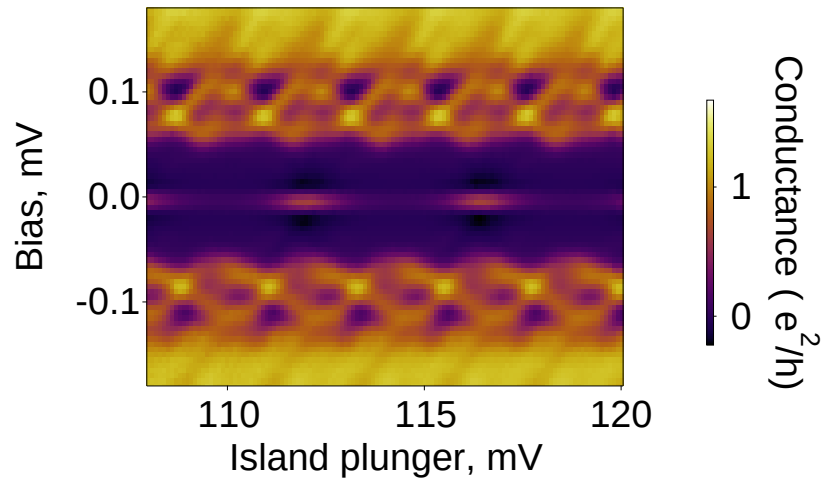

Figure 5.10: Coulomb diamonds of superconducting single dot island.

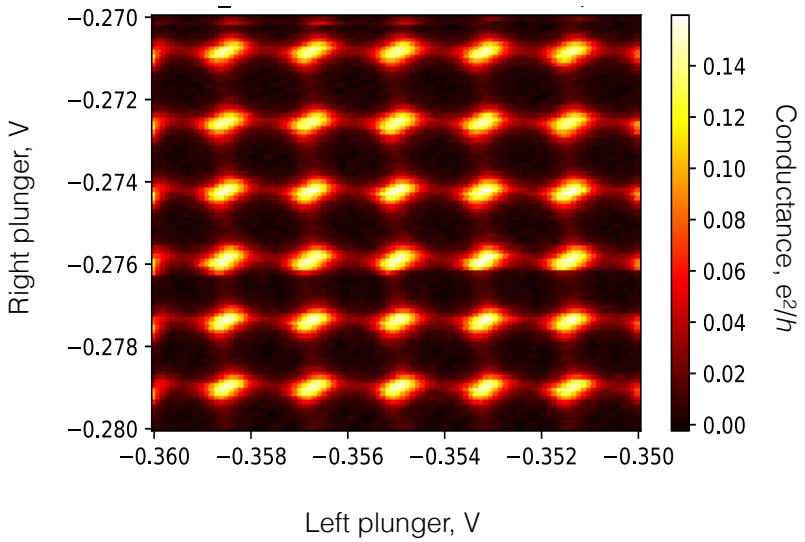

Figure 5.11: Fully decoupled double quantum dot. The merged triple points indicate that the capacitive coupling between the two dots are almost negligible.

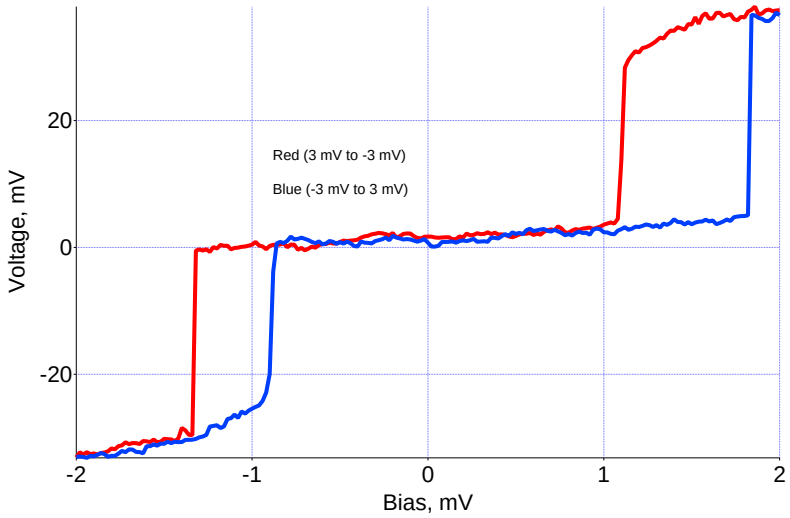

Figure 5.12: Super-current regime in a current biased conductance measurement in a quantum dot regime.

measurement setup. Large bias resistor value ensures that it is this external resistor that defines the current being sourced to the device. Here both forward and backward sweeps are shown. Up to a point where the critical current is reached the junctions forming the QD and the wire itself stays in a super-current branch. When the critical current is reached the island becomes normal and voltage drop is observed. Hysteresis observed in IV traces might be a good indication of Josephson junctions being under-damped.

5.4 Setting up charge sensing

Before we start any measurement that involves charge sensing, be it fast or slow, we need to have a charge sensing set up. Charge sensing is a technique working by a capacitive coupling from the main wire island to the sensor island via a metallic coupler as shown in Figure 5.4. In this way one is able to detect the addition or subtraction of a single electron to or from the QD. The most primitive methodology to check if charge sensing is working would be the

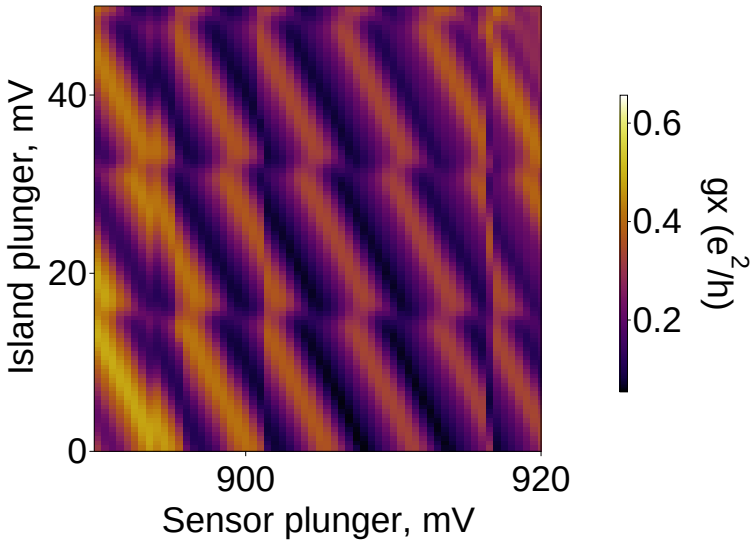

Figure 5.13: Plunger - plunger coupling with a transport measured through the sensor.

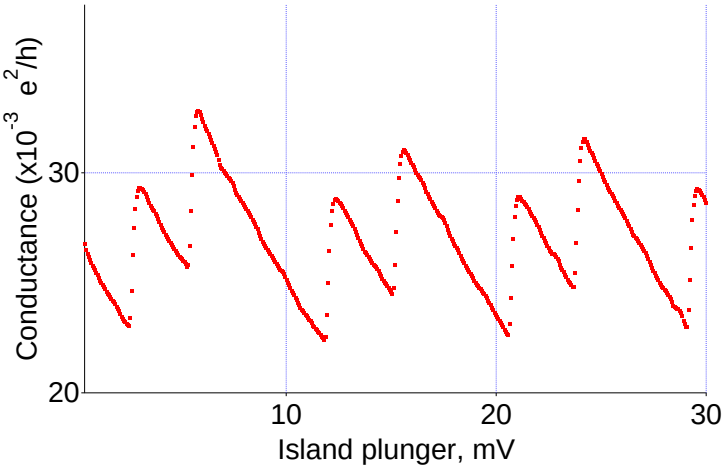

Figure 5.14: Charge sensing step structure as recorded on a sensor when sweeping the main island plunger in the even - odd regime (similar data was reported in [33]).

following:

- if possible, tune both the main NW islands into QD (nice CB dot necessary) and the sensors (not necessary but highly encouraged if possible, as this simplifies setting up charge sensing);

- if tuning sensor into the nice CB dot is not possible, find any "peak" structure that has a slope, as the idea of charge sensing is to sit on a slope of a sensor peak;

- to set up charge sensing one usually starts by making what is known as a plunger - plunger scan. One axis (X) is the sensor plunger voltage and the other (Y) - the plunger voltage of the island NW. When doing this and recording the transport through the sensor in terms of conductance, we arrive at a graph similar to the one shown in Figure 5.13. The step structure in every diagonal line comes from changing the occupation of the QD in the main wire. Every separate diagonal line corresponds to a different charge state in the sensor wire QD, while the slope shows that there is some finite coupling between the two plunger gates.

5.5 Radio frequency charge sensing

In order to get the best sensitivity when using the HF RFL one would have to position himself somewhere on the slope of the CB peak. This is because at that position, the derivative of conductance through the sensor with respect to the gate voltage is the largest, i.e it has the largest slope and, as a result, the sensitivity there is the highest. This means that we have to follow the side of the diagonal line shown in Figure 5.13, as we sweep the plunger of the main island if we want to stay sensitive all the time during the sweep. This is achieved by linearly

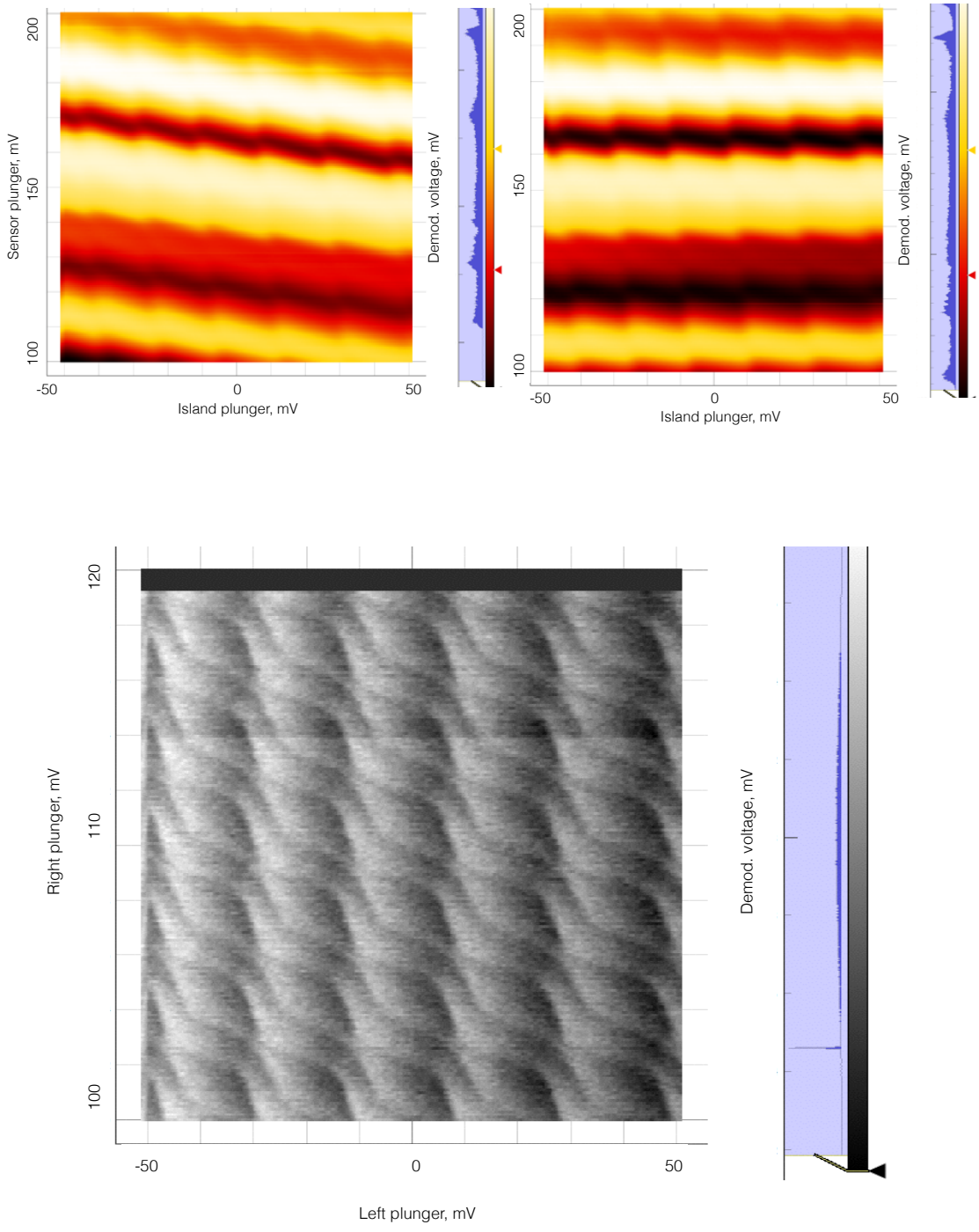

Figure 5.16: Double quantum dot charge stability diagram recorded in fast charge sensing.

changing the sensor plunger as we move the main island plunger. The compensation slope coefficient can be found from the Figure 5.13. When doing FCD measurement as described in the previous chapter where one axis is being ramped at a few kHz frequency while the other slowly stepped one needs to worry about compensating the sensor at the same rate of few kHz since otherwise we would very quickly fall off the CB peak of the sensor. For that one can ramp the sensor plunger with the out of phase sawtooth pattern and with a scaled amplitude in order to compensate the sensor at all times. Example of such a fast compensation technique is shown in Figure 5.15. The left graph shows the non - compensated sensor plunger in fast measurement whereas the right graph shows the fast - compensated version of the same data where the sensor plunger is ramped at the same rate as the main wire plunger. In that case we are able to always stay on the sensor Coulomb peak slope and get the best sensing signal available.

Another illustration is the full charge stability diagram previously called a "wall - wall" diagram recorded in fast charge sensing as shown in Figure 5.16. One axis (x) is ramped at a kHz rate while the other (y) is slowly stepped. Integration time for each data point is around 500 ns and then each line along the x axis is averaged 2000 times. Typical DQD features are clearly seen. This particular tuning was in the even - odd regime on both islands. Only one sensor was used in this case.

5.6 Current and future device geometries

Currently QDev is able to fabricate NW devices with very small E_C (10 *mu*eV - 100 *mu*eV) showing 2e periodic features at zero magnetic field. This is followed by a good quality charge sensing (so far the best achieved result is approximately 2 us of integration time needed to

achieve S/N=1). The main fundamental problem that persists in the current generation of devices is the need for superconducting leads to avoid the 1e normal density of states in the leads and their detrimental interaction to MZM living at 0 bias. This would not be a problem in itself if not the fact that before even starting pulsing for the Majorana based qubit operation one has to identify the MZMs on both superconducting islands and verify their Majorana character. Since initial tuning and characterization is done solely with the help of classical transport LIA measurements it becomes very hard to identify the MZMs sitting at 0 bias. This is due to the blocked transport at 0 bias due to SC leads. Hence being able to probe the DOS with the trivial instead of SC leads would be a huge advantage. Another problem is more of an engineering one: to find a regime in which the DQD can be moved from an open E_J dominated regime to closed E_C dominated regime without hitting any unwanted resonances usually formed by accidental QDs due to improper etching or just band bending. The classical Aasen et al. qubit as outlined in [31] suffer from the fact that the two inner MZMs are too near each other and any noise on the middle cutter might be detrimental to the splitting of two MZMs controlled by that cutter. One possible solution to this problem is shown in 5.17 where a so called tetron qubit design is sketched. The idea here is to add two additional plungers around the middle cutter to protect the inner MZMs by the hard gap trivial SC around the middle cutter. In this particular geometry the outer cutters would stay closed throughout the full cycle of the experiment and only the middle cutter needs to be pulsed on and off the interaction of two inner MZMs. Having outer cutters closed all the time brings a small disadvantage - E_C however small, is always present in the system. This means that we are allowing some residual splitting and rotation on a Bloch sphere given by the E_C. The advantage of the design shown in Figure 5.17 is threefold:

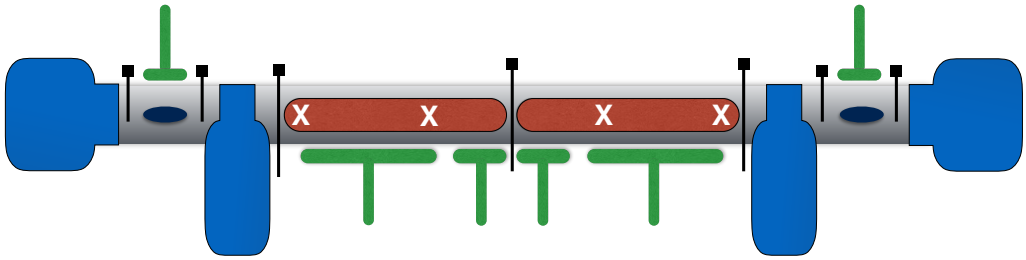

Figure 5.17: Design drawing of the Majorana qubit. Grey is the InAs nanowire, red - un-etched Al, blue - golden leads, green - plunger gates controlling the electron density in the wire and tuning the Coulomb oscillations in a quantum dot regime, black - cutter gates forming tunnel barriers, yellow - capacitive coupler between the two islands.

- firstly, in this geometry we get a four - probe geometry for the main wire for free if needed since the inner leads can be easily used for the voltage drop measurement whereas the outer leads for injecting the current;

- secondly, given how many devices before were found to be not working or blown away before even starting the measurements, here only four instead of six ohmic contacts are needed to be working, hence statistically 33% bigger success rate;

- finally, this geometry helps in finding the MZMs before moving to sensing and to the Majorana qubit in general. Since these devices have normal leads instead of superconducting it directly allows the celebrated N - I - S spectroscopy to be used for probing the MZMs potentially present on both sides. This is easier than with the superconducting leads because here one is not bothered by the convolution of two superconducting gaps as in S - I - S geometry and any other bound states that are not MZMs and that are probed S - I - S geometry. Having N - I - S geometry is simpler since in a tunneling regime it give a signature (differential conductance in our case) that is directly propor-

tional to the density of states in the superconducting part. In the MZM case it would show up as a ZBP instead of Δ, 0, or $-\Delta$ bias features in S - I - S geometry which so far were hard to notice in our devices.

There are also few disadvantages nevertheless:

- firstly, there is no proper combination of excitation and detection geometry if one wants to measure both the main wire and two sensors simultaneously using slow LIA techniques. This is because the current through the main wire is always affected by the state of the sensor and vice versa. The best way to characterize the island and one of the sensors simultaneously would be to float one of the outer leads of one of the sensors. Then we can put the excitation on one of the inner leads and detection with two different synced to the same frequency LIAs on the outer outer lead and the other inner lead. In this case the measurement setup even though still not perfect but at least allows some useful information to be gained about the main island and the sensor simultaneously;

- other thing which we thought would be a disadvantage initially but turned out not to be is the fact that the two different RFL frequencies would "speak" with each other from the two different outer ends of the device where RFL circuits are connected. However after testing the fast sensing on this device we noticed that sensors act independently and no obvious distortion coming from the first TC was seen in the second TC and vice versa. In conclusion if one moves to purely characterizing the device in fast sensing with the outer cutters shut it does not matter if the sensors are fabricated on the same wire or on two different wires.

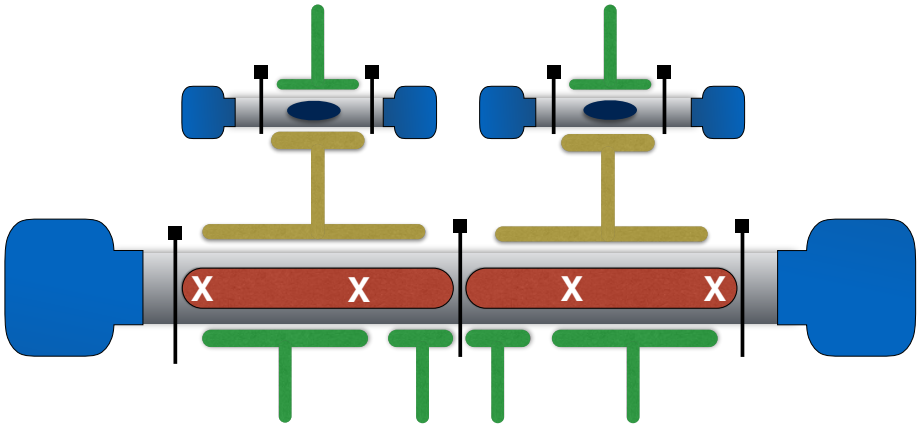

Figure 5.18: Design drawing of the Majorana qubit. Grey is the InAs nanowire, red - un-etched Al, blue - golden leads, green - plunger gates controlling the electron density in the wire and tuning the Coulomb oscillations in a quantum dot regime, black - cutter gates forming tunnel barriers, yellow - capacitive coupler between the two islands.

It is also worth mentioning that the design of the device presented above is only feasible given that the length of the NW is sufficient to add the sensors at its ends. If this is not the case one can put the sensors nearby on two separate Al - free NWs as in the original design. For that to be solved in the next generation of devices we are planning to move back to the sensors being on the separate nearby wires instead of on the same wire, see Fig 5.17. The cut - tetron qubit operation outlined above would be very similar to the traditional Aasen et al.[31] qubit operation as also outlined in [49,50]:

- In the first stage, the whole wire is in the topological superconducting regime with four MZMs present in the system;
- In the second stage, the middle cutter is opened for some time to allow some hybridization between the two inner MZMs;
- In the final stage, the tetron is again cut in the middle and the charge on both islands is measured.

In principle given that there is no poisoning it is enough to measure only one of the sides only. Since the total parity is conserved this effectively measures the other side as well. As already mentioned the advantage of this geometry compared to traditional Aasen et al. qubit is that the cut - tetron is always disconnected from the environment since the outer cutters are always closed. In that case we win N - I - S geometry for probing MBSs in an easier way but have to avoid superconducting leads expecting that always closed outer cutters will minimize the quasi - particle poisoning from the normal leads.

5.7 Towards Majorana - Cooper pair box qubit

If one stays at zero magnetic field, the devices presented in principle could act as a E_J tunable charge qubit - CPB, similarly as in[39]. The idea would be to close one of the outer cutters, for example the left cutter in Fig 5.17. Then the most right cutter would be open or partially closed whereas the middle cutter would control the E_J coupling with the reservoir on the right. The anti - crossing between the two charge states given by the middle cutter value would in principle create a two level system. Then after applying the square pulse on the plunger that would pulse the system to degeneracy, let it evolve there for some time and then pulse back. In principle this allows to observe the coherent oscillations between the two charge states if we vary the waiting time at the degeneracy. The advantage of this particular device geometry compared to the one in[39] is that here we in principle have a knob on E_J value which let us tune the frequency of oscillations whereas in previous works it was fixed and could not be tuned.

Recently a new and a very naive and bold idea was set up together with my collaborator which would allow 2e periodic CPB to show 1e periodic coherent oscillations. It is important

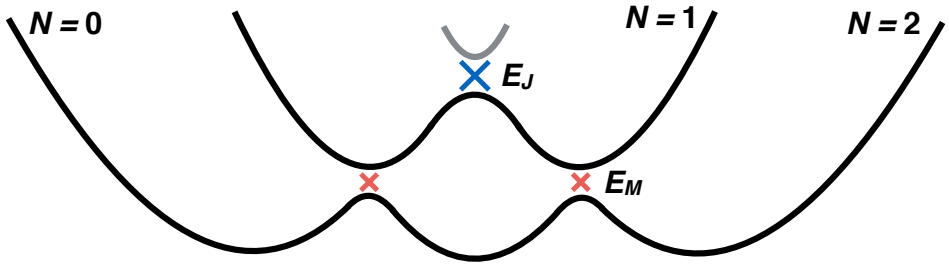

Figure 5.19: Majorana - assisted Cooper pair box energy diagram.

to mention that this qubit is in no way topologically protected. However given MFs really exist in our system they should give a 1e periodic behavior in a pulsing experiment i.e. would demonstrate the coherent control of 1e topological charge states. This idea was somewhat inspired by the work done by Nakamura et al. Even though exact details of this experiment remains to be worked out below I present the most simple schematics of the energy diagram of the system in the 1e operational regime, see Figure 5.19.

The idea for the experiment is the following. Given that we are in the topological regime, the superconducting QD is formed where one barrier is shut down and the other acts as the E_J controlling barrier. The barrier that controls E_J introduces the anti - crossing both between the 2e Cooper pair states, as well as the coupling between the 1e MZM states with the latter given by the overlap of two MZMs from two different sides of the E_J controlling barrier. Coherent superposition of 2e charge states are created by pulsing the plunger of the CPB from the valley between the Cooper pair degeneracy points to the Cooper pair degeneracy using the fast plunger gate. After unitary time evolution, the box state is pulsed back. This projects the

superposition state onto the ground or exited state. The exited charge state relaxes to the ground state over some characteristic time by the ejection of two electrons into the probe lead, almost exactly like in Nakamura et. al original paper[39]. This generates a current which is directly proportional to the probability that the box was in the excited state.

Very similarly we would like to read and detect an "excited" 1e Majorana state in the topological regime. However here we would use the anti - crossing between 1e charge states, which is introduced by the coupling of MZMs on both sides of the middle cutter. What Nakamura was lacking 20 years ago with his simple Al island we have under full control: tunable E_J. In principle one could take advantage of the tunable E_J when in need to discriminate between trivial Andreev states and MBS. The idea would be to look at the critical current dependence on the transparency of the barrier defined by the middle cutter. In the trivial Andreev bound state case it should scale differently compared to MBS case and that could potentially help to discriminate between the two cases.

Lectures which really teach will never be popular; lectures which are popular will never really teach.

Michael Faraday

6

Conclusion and discussion

This work concerned with the measurements and characterization of the superconducting single and double quantum dot islands in one dimensional system. I presented the notions of quantum information and topological quantum computing, basic steps needed for fabricating the nanowire devices, low temperature techniques used in the experiments, fast data acquisition setup and characterization of the devices in transport and fast sensing. The devices used in the experiment consists of an InAs nanowire with an epitaxially grown 2-facet Al shell lithographically patterned into two superconducting islands. Fast readout is performed using the reflectometry technique using a second proximal nanowire functioning as the charge sensor. Currently it is possible to fabricate NW devices with the very small E_C showing 2e periodic features at zero magnetic field as well as very good quality charge sensing allowing nearly single shot readout. Since initial tuning and characterization is done solely with the help of classical transport lock - in measurements the main problem that still persists in the current set of devices is the ability to uniquely identify the topological regime and Majorana zero modes present in the system. So far this has been the biggest problem but hopefully will be easily solved with the new generation of devices allowing direct N - I - S spectroscopy to be used to probe the Majorana zero modes when looking at 0 bias features. Data coming from the first N - I - S spectroscopy allowing devices looks very promising indicating that very soon we will be able to probe and identify the Majorana zero modes presence on the islands with the very high fidelity. Then equipped with the expertise in fast pulsing and fast measurements it should hopefully not take to long to realize the first ever demonstration of coherent oscillations in Majorana assisted qubit.

A

List of Abbreviations

A

- AC - Alternating current
- ALD - Atomic layer deposition
- Al - Aluminum
- AWG - Arbitrary waveform generator

B

- BCS - Bardeen - Cooper - Schriefer
- BG - Backgate
- BW - Bandwidth

C

- CB - Coulomb blockade
- CPB - Cooper pair box

D

- DAC - Digital - to - analog converter

- DC - Direct current
- DGHTB - Daughterboard
- DOS - Density of states
- DQD - Double quantum dot

E

- EBL - Electron beam lithography
- E_C - Charging energy
- E_J - Josephson energy

F

- FCD - Fast charge diagrams

G

- GND - ground

H

- HF - High frequency

I

- InAs - Indium arsenide

L

- LF - Low frequency
- LIA - Lock - in amplifier
- LT - Low temperature
- LRC - Resonant circuit made out of inductor, resistor and capacitor

M

- MBE - Molecular beam epitaxy
- MBS - Majorana bound state
- MC - Mixing Chamber
- MF - Majorana fermion
- MO - Majorana operator
- MTHB - Motherboard
- MZM - Majorana zero mode

N

- N - I - S - Normal metal - insulator - superconductor
- NW - Nanowire

Q

- QCoDeS - Data acquisition software
- QD - Quantum Dot
- QDEV - Center for Quantum Devices
- QIP - Quantum information processing
- QP - Quasi - particle

R

- RF - Radio frequency
- RFL - Reflectometry

S

- SC - Superconductor

- SEM - Scanning electron microscope
- SmC - Semiconductor
- SNR - Signal - to - noise ratio
- SO - Spin - orbit coupling
- Si - Silicon

T

- TC - Tank circuit
- TS - Topological superconductor

U

- UHFLI - Ultra high frequency lock-in

W

- WF - Wavefunction

Z

- ZBP - Zero bias peak
- ZI - Zurich instruments

B

Pin-out schematics for fast lines

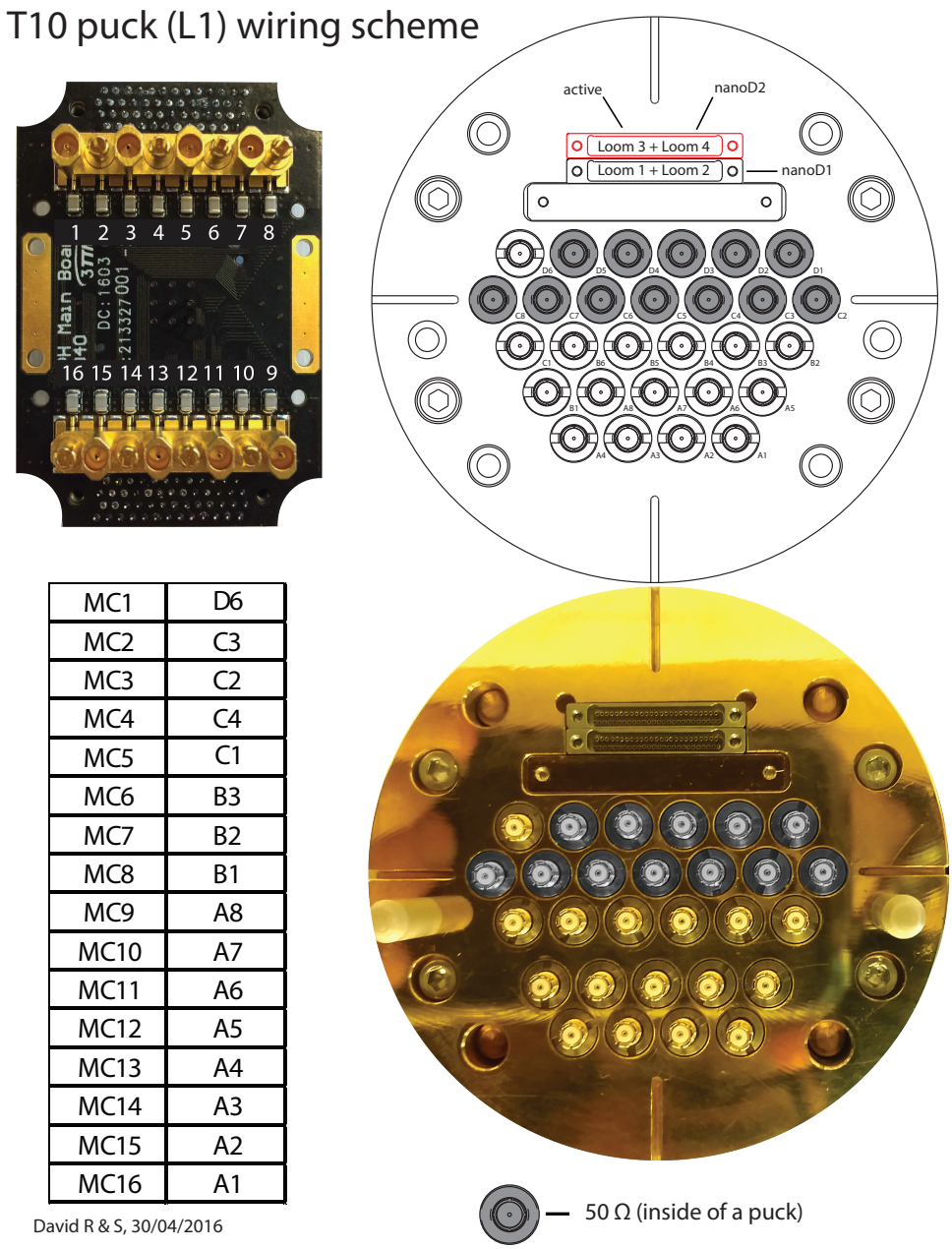

MC1	D6
MC2	C3
MC3	C2
MC4	C4
MC5	C1
MC6	B3
MC7	B2
MC8	B1
MC9	A8
MC10	A7
MC11	A6
MC12	A5
MC13	A4
MC14	A3
MC15	A2
MC16	A1

David R & S, 30/04/2016

Figure B.1: Puck RF wiring scheme. Shown are radio frequency lines mapping from the inside of the puck to the outside of the dilution refrigerator.

References

[1] Michael A Nielsen and Isaac L Chuang. *Quantum computation and quantum information*. Cambridge university press, 2010.

[2] Peter W Shor. Polynomial-time algorithms for prime factorization and discrete logarithms on a quantum computer. *SIAM review*, 41(2):303–332, 1999.

[3] L DiCarlo, JM Chow, JM Gambetta, Lev S Bishop, BR Johnson, DI Schuster, J Majer, A Blais, L Frunzio, SM Girvin, et al. Demonstration of two-qubit algorithms with a superconducting quantum processor. *Nature*, 460(7252):240–244, 2009.

[4] Lieven MK Vandersypen, Matthias Steffen, Gregory Breyta, Costantino S Yannoni, Mark H Sherwood, and Isaac L Chuang. Experimental realization of shor's quantum factoring algorithm using nuclear magnetic resonance. *Nature*, 414(6866):883–887, 2001.

[5] Matteo Mariantoni, H Wang, T Yamamoto, M Neeley, Radoslaw C Bialczak, Y Chen, M Lenander, Erik Lucero, AD O'connell, D Sank, et al. Implementing the quantum von neumann architecture with superconducting circuits. *Science*, 334(6052):61–65, 2011.

[6] David P DiVincenzo et al. The physical implementation of quantum computation. *arXiv preprint quant-ph/0002077*, 2000.

[7] David P DiVincenzo. Quantum computation. *Science*, 270(5234):255, 1995.

[8] Emanuel Knill, Raymond Laflamme, and Gerald J Milburn. A scheme for efficient quantum computation with linear optics. *nature*, 409(6816):46–52, 2001.

[9] Ettore Majorana. Teoria simmetrica dell'elettrone e del positrone. *Il Nuovo Cimento (1924-1942)*, 14(4):171–184, 1937.

[10] Paul AM Dirac. The quantum theory of the electron. In *Proceedings of the Royal Society of London A: Mathematical, Physical and Engineering Sciences*, volume 117, pages 610–624. The Royal Society, 1928.

[11] Steven R Elliott and Marcel Franz. Colloquium: Majorana fermions in nuclear, particle, and solid-state physics. *Reviews of Modern Physics*, 87(1):137, 2015.

[12] Martin Leijnse and Karsten Flensberg. Introduction to topological superconductivity and majorana fermions. *Semiconductor Science and Technology*, 27(12):124003, 2012.

[13] Frank Wilczek. Majorana returns. *Nature Physics*, 5(9):614–618, 2009.

[14] Chetan Nayak, Steven H Simon, Ady Stern, Michael Freedman, and Sankar Das Sarma. Non-abelian anyons and topological quantum computation. *Reviews of Modern Physics*, 80(3):1083, 2008.

[15] Tudor D Stanescu and Sumanta Tewari. Majorana fermions in semiconductor nanowires: fundamentals, modeling, and experiment. *Journal of Physics: Condensed Matter*, 25(23):233201, 2013.

[16] A Yu Kitaev. Fault-tolerant quantum computation by anyons. *Annals of Physics*, 303(1):2–30, 2003.

[17] A Yu Kitaev. Unpaired majorana fermions in quantum wires. *Physics-Uspekhi*, 44(10S):131, 2001.

[18] A. Cook and M. Franz. Majorana fermions in a topological-insulator nanowire proximity-coupled to an *s*-wave superconductor. *Phys. Rev. B*, 84:201105, Nov 2011.

[19] Roman M. Lutchyn, Jay D. Sau, and S. Das Sarma. Majorana fermions and a topological phase transition in semiconductor-superconductor heterostructures. *Phys. Rev. Lett.*, 105:077001, Aug 2010.

[20] Yuval Oreg, Gil Refael, and Felix von Oppen. Helical liquids and majorana bound states in quantum wires. *Phys. Rev. Lett.*, 105:177002, Oct 2010.

[21] Jason Alicea. Majorana fermions in a tunable semiconductor device. *Physical Review B*, 81(12):125318, 2010.

[22] Jay D Sau, Sumanta Tewari, Roman M Lutchyn, Tudor D Stanescu, and S Das Sarma. Non-abelian quantum order in spin-orbit-coupled semiconductors: Search for topological majorana particles in solid-state systems. *Physical Review B*, 82(21):214509, 2010.

[23] Jay D Sau, Roman M Lutchyn, Sumanta Tewari, and S Das Sarma. Generic new platform for topological quantum computation using semiconductor heterostructures. *Physical review letters*, 104(4):040502, 2010.

[24] Jason Alicea, Yuval Oreg, Gil Refael, Felix von Oppen, and Matthew PA Fisher. Non-abelian statistics and topological quantum information processing in 1d wire networks. *Nature Physics*, 7(5):412–417, 2011.

[25] Jay D Sau, David J Clarke, and Sumanta Tewari. Controlling non-abelian statistics of majorana fermions in semiconductor nanowires. *Physical Review B*, 84(9):094505, 2011.

[26] Liang Fu and Charles L Kane. Superconducting proximity effect and majorana fermions at the surface of a topological insulator. *Physical review letters*, 100(9):096407, 2008.

[27] Vincent Mourik, Kun Zuo, Sergey M Frolov, SR Plissard, EPAM Bakkers, and LP Kouwenhoven. Signatures of majorana fermions in hybrid superconductor-semiconductor nanowire devices. *Science*, 336(6084):1003–1007, 2012.

[28] MT Deng, CL Yu, GY Huang, Marcus Larsson, Philippe Caroff, and HQ Xu. Anomalous zero-bias conductance peak in a nb–insb nanowire–nb hybrid device. *Nano letters*, 12(12):6414–6419, 2012.

[29] Leonid P Rokhinson, Xinyu Liu, and Jacek K Furdyna. The fractional ac josephson effect in a semiconductor-superconductor nanowire as a signature of majorana particles. *Nature Physics*, 8(11):795–799, 2012.

[30] Anindya Das, Yuval Ronen, Yonatan Most, Yuval Oreg, Moty Heiblum, and Hadas Shtrikman. Zero-bias peaks and splitting in an al-inas nanowire topological superconductor as a signature of majorana fermions. *Nature Physics*, 8(12):887–895, 2012.

[31] David Aasen, Michael Hell, Ryan V. Mishmash, Andrew Higginbotham, Jeroen Danon, Martin Leijnse, Thomas S. Jespersen, Joshua A. Folk, Charles M. Marcus, Karsten Flensberg, and Jason Alicea. Milestones toward majorana-based quantum computing. *Phys. Rev. X*, 6:031016, Aug 2016.

[32] Brian David Josephson. Possible new effects in superconductive tunnelling. *Physics letters*, 1(7):251–253, 1962.

[33] Deividas Sabonis. Controlling superconductor-semiconductor quantum dots: Towards single shot readout of majorana zero modes in inas/al nanowires. *TU Munich*, 2016.

[34] P Krogstrup, NLB Ziino, W Chang, SM Albrecht, MH Madsen, Erik Johnson, Jesper Nygård, CM Marcus, and TS Jespersen. Epitaxy of semiconductor–superconductor nanowires. *Nature materials*, 14(4):400–406, 2015.

[35] W Chang, SM Albrecht, TS Jespersen, Ferdinand Kuemmeth, P Krogstrup, J Nygård, and CM Marcus. Hard gap in epitaxial semiconductor–superconductor nanowires. *Nature nanotechnology*, 10(3):232–236, 2015.

[36] So Takei, Benjamin M. Fregoso, Hoi-Yin Hui, Alejandro M. Lobos, and S. Das Sarma. Soft superconducting gap in semiconductor majorana nanowires. *Phys. Rev. Lett.*, 110:186803, Apr 2013.

[37] Tudor D. Stanescu and S. Das Sarma. Superconducting proximity effect in semiconductor nanowires. *Phys. Rev. B*, 87:180504, May 2013.

[38] Robert Coleman Richardson and Eric N Smith. *Experimental techniques in condensed matter physics at low temperatures*. Addison-Wesley Redwood City, CA, 1988.

[39] Y Nakamura, YA Pashkin, and JS Tsai. Coherent control of macroscopic quantum states in a single-cooper-pair box. 1999.

[40] RJ Schoelkopf, P Wahlgren, AA Kozhevnikov, P Delsing, and DE Prober. The radio-frequency single-electron transistor (rf-set): a fast and ultrasensitive electrometer. *Science*, 280(5367):1238–1242, 1998.

[41] DJ Reilly, CM Marcus, MP Hanson, and AC Gossard. Fast single-charge sensing with a rf quantum point contact. *Applied Physics Letters*, 91(16):162101, 2007.

[42] Christian Barthel, Morten Kjærgaard, J Medford, Michael Stopa, Charles Masamed Marcus, MP Hanson, and Arthur C Gossard. Fast sensing of double-dot charge arrangement and spin state with a radio-frequency sensor quantum dot. *Physical Review B*, 81(16):161308, 2010.

[43] M Jung, MD Schroer, KD Petersson, and JR Petta. Radio frequency charge sensing in inas nanowire double quantum dots. *Applied Physics Letters*, 100(25):253508, 2012.

[44] MC Cassidy, AS Dzurak, RG Clark, KD Petersson, I Farrer, DA Ritchie, and CG Smith. Single shot charge detection using a radio-frequency quantum point contact. *Applied Physics Letters*, 91(22):222104, 2007.

[45] AJ Ferguson, FE Hudson, RG Clark, et al. Microsecond resolution of quasiparticle tunneling in the single-cooper-pair transistor. *Physical review letters*, 97(10):106603, 2006.

[46] Silvano De Franceschi, Leo Kouwenhoven, Christian Schönenberger, and Wolfgang Wernsdorfer. Hybrid superconductor-quantum dot devices. *Nature Nanotechnology*, 5(10):703–711, 2010.

[47] GE Blonder, M Tinkham, and TM Klapwijk. Transition from metallic to tunneling regimes in superconducting microconstrictions: Excess current, charge imbalance, and supercurrent conversion. *Physical Review B*, 25(7):4515, 1982.

[48] Michael Tinkham. *Introduction to superconductivity*. Courier Corporation, 1996.

[49] Michael Hell, Jeroen Danon, Karsten Flensberg, and Martin Leijnse. Time scales for majorana manipulation using coulomb blockade in gate-controlled superconducting nanowires. *Phys. Rev. B*, 94:035424, Jul 2016.

[50] Liang Fu and C. L. Kane. Superconducting proximity effect and majorana fermions at the surface of a topological insulator. *Phys. Rev. Lett.*, 100:096407, Mar 2008.